

1 **Multi-element dataset of soil profiles across climatic zones in China's mountains**

2 Yuying Wu <sup>a,b</sup>, Yuhan Wang <sup>a,c</sup>, Wenzheng Yang <sup>a</sup>, Jie Zhang <sup>a</sup>, Yanhong Wu <sup>a</sup>, Jun Li <sup>d</sup>, Gan Zhang <sup>d</sup>,

3 Haijian Bing <sup>a,\*</sup>

4 <sup>a</sup> Institute of Mountain Hazards and Environment, Chinese Academy of Sciences, Chengdu 610213,

5 China

6 <sup>b</sup> University of Chinese Academy of Sciences, Beijing 10049, China

7 <sup>c</sup> Key Laboratory of Green Utilization of Critical Non-metallic Mineral Resources, Ministry of Education,

8 Wuhan University of Technology, Wuhan 430070, China

9 <sup>d</sup> State Key Laboratory of Organic Geochemistry, Guangzhou Institute of Geochemistry, Chinese

10 Academy of Sciences, Guangzhou 510640, China

11  
12 \* Corresponding author:

13 Haijian Bing (PhD), E-mail: [hjbing@imde.ac.cn](mailto:hjbing@imde.ac.cn)

14

15 **Abstract**

16 **Datasets of soil multi-element concentrations are essential for advancing our understanding of ecological**  
17 **functioning and responses to global change in mountain regions. However, the paucity of such datasets**  
18 **represents a fundamental impediment to accurately assess and predict biogeochemical processes in these**  
19 **sensitive ecosystems.** Here, we present a comprehensive geochemical dataset comprising more than  
20 1,300 soil samples collected from 166 sites across 30 mountain regions in China, spanning five major  
21 climatic zones and representative vegetation types. Soil samples were systematically collected from three  
22 standardized horizons (organic, surface mineral, and parent material), and analyzed for the concentrations  
23 of 24 elements, including macronutrients (e.g., phosphorus, potassium, calcium, magnesium),  
24 micronutrients (e.g., iron, molybdenum, manganese, copper), and trace metals (e.g., cadmium, chromium,  
25 lead, antimony). To support integrated Earth system analyses, the dataset is accompanied by key site-  
26 specific environmental variables, including climate parameters (temperature, precipitation, aridity index),  
27 normalized difference vegetation index, soil physicochemical properties (pH, moisture, bulk density),  
28 soil type, parent rock type, atmospheric nitrogen deposition, and chemical index of alteration. The dataset  
29 reveals significant vertical stratification in element distributions, with organic horizon enriched in  
30 biogenic elements, and deeper horizons dominated by lithogenic components. Spatial patterns along  
31 latitudinal, longitudinal, and altitudinal gradients underscore the influence of climate and geology on soil  
32 chemistry. This open-access dataset provides a valuable resource for parameterizing and validating  
33 biogeochemical models, assessing soil quality in mountain regions, and improving predictions of  
34 ecosystem responses to global change. The dataset can be accessed via  
35 <https://doi.org/10.11888/Terre.tpd.302620> or <https://cstr.cn/18406.11.Terre.tpd.302620> (Wu et al.,  
36 2025b).

37 **Key words:** Mountain ecosystems, Soil dataset, Elementome, Soil profile, Multi-elements

## 38 **1 Introduction**

39 Mountain ecosystems, recognized globally as hotspots of biodiversity and critical regulators of Earth's  
40 biogeochemical cycles, are under increasing pressure from accelerating global changes ([Antonelli et al.,](#)  
41 [2018](#); [Wang et al., 2022](#)) and anthropogenic impacts. The complex topography of mountain regions  
42 creates steep climatic and edaphic gradients over short spatial distances, generating distinct  
43 biogeochemical niches that are highly sensitive to environmental change ([Dainese et al., 2024](#); [Nogués-](#)  
44 [Bravo, 2007](#)). Soils in these regions are central to ecosystem functioning, supporting primary productivity,  
45 nutrient cycling, and carbon sequestration ([Cui et al., 2022](#); [Sundqvist et al., 2013](#)). However, our  
46 understanding of how these functions are regulated by the distribution and interaction of multiple soil  
47 elements remains limited, particularly under conditions of rapid global change ([Kaspari and Powers,](#)  
48 [2016](#); [Tian et al., 2019](#); [Wu et al., 2025a](#)). A fundamental constraint hindering progress in this field is the  
49 scarcity of comprehensive, large-scale datasets that simultaneously quantify the distribution and  
50 interaction of a wide range of soil elements across diverse mountain landscapes. Overcoming this data  
51 deficiency is essential for unraveling the emergent properties of coupled biogeochemical cycles in these  
52 vulnerable ecosystems and for developing robust predictive models for their future integrity and  
53 resilience.

54 While the roles of key elements such as carbon (C) and phosphorus (P) in ecosystem processes are  
55 well established ([Elser et al., 2010](#); [Zuo et al., 2024](#); [Wang et al., 2024](#)), recent research highlights the  
56 importance of a broader suite of elements, including macronutrients, micronutrients, and trace metals, in  
57 shaping biogeochemical dynamics ([Han et al., 2011](#); [Vallicrosa et al., 2022](#)). For instance, calcium (Ca),  
58 magnesium (Mg), and potassium (K) are essential for plant physiological processes ([Fernández-Martínez](#)  
59 [et al., 2021](#); [Peñuelas et al., 2019](#)), while micronutrients such as molybdenum (Mo), copper (Cu), and  
60 manganese (Mn) function as critical cofactors in enzymatic pathways driving nitrogen fixation, methane  
61 oxidation, and organic matter decomposition ([Dai et al., 2023](#); [Hay et al., 2023](#)). Furthermore, the  
62 intricate interplay between trace element availability and the structure and function of microbial  
63 communities is increasingly recognized as a key control on soil biogeochemistry ([Giovannelli, 2023](#);  
64 [Shafiee et al., 2021](#); [Zhao et al., 2020](#)). Conversely, elevated concentrations of toxic elements, including  
65 aluminum (Al), cadmium (Cd), chromium (Cr), and lead (Pb), can disrupt ecosystem integrity and impair  
66 ecosystem health through food chain transfer ([Bing et al., 2016](#); [Lynch and St. Clair, 2004](#); [Nagajyoti et](#)

67 [al., 2010](#)). Capturing the distribution and interactions of this wide range of elements is therefore  
68 indispensable for a mechanistic understanding of mountain ecosystem functioning ([Fernández-Martínez](#)  
69 [et al., 2021](#); [Kaspari and Powers, 2016](#); [Vallicrosa, 2022](#)).

70 Emerging evidence suggests that the composition and distribution of soil elements are regulated not  
71 only by individual environmental drivers such as climate, vegetation, and parent material, but also by  
72 complex interactions among these factors ([Augusto et al., 2017](#); [Haghverdi et al., 2019](#); [Molina et al.,](#)  
73 [2024](#); [Moreno-Jiménez et al., 2022](#)). These interactions can lead to non-linear responses and threshold  
74 effects that are difficult to predict without comprehensive, spatially explicit datasets ([Feng et al., 2024](#)).  
75 Vertical stratification of elements along soil profiles further reflects the combined influence of biological  
76 inputs, weathering processes, and leaching losses, offering insights into long-term ecosystem  
77 development and nutrient cycling ([Cronan et al., 2018](#); [Kirkby, 2018](#); [Jobbágy and Jackson, 2001](#);  
78 [Steinnes and Lierhagen, 2018](#)). For instance, biologically cycled elements tend to accumulate in organic-  
79 rich layers, while lithogenic elements are often more concentrated in deeper mineral layers or parent  
80 material ([Jobbágy and Jackson, 2004](#); [Agnan et al., 2019](#); [Sayer et al., 2020](#)). However, few studies have  
81 captured this vertical dimension across broad environmental gradients, and most existing datasets are  
82 limited in geographic scope, sampling depth, or the range of elements analyzed ([Moreno-Jiménez et al.,](#)  
83 [2019](#); [Ochoa-Hueso et al., 2023](#); [Shangguan et al., 2014](#)).

84 China's extensive and environmentally diverse mountain systems, which cover over two-thirds of  
85 the nation's terrestrial area, offer an exceptional natural laboratory for dissecting the complex interactions  
86 among climate, vegetation, geology, and soils that shape global biogeochemical cycles ([Han et al., 2011](#)).  
87 These mountains span a wide range of climatic zones, from tropical and subtropical rainforests to  
88 temperate forests, boreal forests, and alpine tundra, nearly including the full spectrum of Earth's  
89 terrestrial biomes ([Kou et al., 2021](#); [Lu et al., 2018](#)). The combination of steep altitudinal gradients, varied  
90 parent materials, and diverse vegetation types results in a mosaic of soil environments that mirrors the  
91 global diversity of pedogenic conditions. Critically, many of these mountain regions remain relatively  
92 undisturbed by direct anthropogenic activities, providing a unique opportunity to assess natural controls  
93 on soil geochemistry and to establish baselines for detecting future environmental change. Here, we  
94 conducted a large-scale soil sampling campaign across 30 mountain ecosystems in China. These sites  
95 represent five major climatic zones and typical vegetation types in each region. A total of 1,314 soil

96 samples were collected from three standardized soil horizons (organic (O), surface mineral (A), and  
97 parent material (C)). Each sample was analyzed for the concentrations of 24 elements, including  
98 macronutrients, micronutrients, and trace metals. In addition, the dataset was integrated with a suite of  
99 ancillary variables, including satellite-derived vegetation indices, soil physicochemical properties, and  
100 climatic parameters. This dataset provides a rare, high-resolution view of multi-element distributions  
101 across spatial and vertical gradients in mountain soils. It enables cross-disciplinary analyses that link  
102 geochemical, ecological, and climatic processes, and serves as a critical resource for improving  
103 biogeochemical modeling, evaluating soil quality and ecosystem health, and understanding the resilience  
104 of mountain systems under global change.

## 105 **2 Materials and methods**

### 106 **2.1 Study area**

107 Soil samples were collected from 30 mountains located within accessible national and provincial nature  
108 reserves across China (Fig. 1). The study area spans a wide geographical range (18.9°N-53.5°N, 101.0°E-  
109 129.6°E, altitude: 210-4225 m above sea level). These sites represent diverse ecosystem zones, including  
110 tropical, subtropical, warm temperate, temperate, and cold temperate regions. Vegetation types include  
111 broadleaf forests, mixed broadleaf-coniferous forests, coniferous forests, and shrublands (Bing et al.,  
112 2021; Cui et al., 2022). The mean annual temperature (MAT) in the study area ranges between -5°C and  
113 21°C, and the mean annual precipitation (MAP) varies between 223 mm and 1934 mm. Detailed  
114 information in each mountain can be found in Table 1.

### 115 **2.2 Soil sampling**

116 **Sampling campaigns were conducted at 166 sites spanning 30 mountains between July 2012 and March**  
117 **2013.** In each mountain, sites were selected based on the altitude and dominant vegetation types. At each  
118 site, the geographic coordinate was recorded using a GPS device (eTrex Venture, USA). **Three replicate**  
119 **plots (10 m × 10 m) were randomly established per site, spaced approximately 50 m apart to account for**  
120 **spatial heterogeneity. In each plot, soil profiles were manually excavated down to the parent material**  
121 **horizon.** Soil horizons were delineated in the field based on morphological characteristics following the  
122 Chinese Soil Taxonomy (Chinese Soil Taxonomy Research Group, 2001; Yang et al., 2023). Horizon  
123 boundaries were determined through visual and tactile assessments (e.g., color, texture, consistency,  
124 moisture, and root distribution). Horizons were typically classified as O (organic), A (surface mineral),

125 and C (parent material) horizons. For each profile, the name, code, depth range, and diagnostic features  
126 were recorded. Soil samples were collected sequentially from bottom to up within each profile to avoid  
127 cross-pollution, with composite samples formed by homogenizing subsamples from each horizon.  
128 Samples were preserved in clean and sealed polyethylene bags and transported to the laboratory. A total  
129 of 1314 samples were obtained, comprising 381 from O horizon, 481 from A horizon, and 452 from C  
130 horizon. The limited pedogenic development in some mountain soils resulted in the absence of certain  
131 horizons in profiles. All samples were air-dried, and visible roots, litter, coarse fragments, and other  
132 debris were manually removed. The soils were then sieved through a 2 mm mesh prior to further analyses.  
133 At each sampling site, bulk density (BD) measurements were conducted adjacent to a representative soil  
134 profile. For mineral horizons, BD was determined using the standard cylindrical core method with  
135 stainless-steel rings. However, BD of the typically thin, organic-rich O horizon was measured by  
136 excavating pits of known volume. The volume of the excavated soils was quantified via water  
137 displacement by backfilling the pits (Maynard and Curran, 2007).

### 138 2.3 Soil physical and chemical analyses

139 Soil moisture content was determined by oven-drying the soils at 105°C to constant mass, which was  
140 calculated using the following formula:

$$141 \text{ Moisture (\%)} = \frac{\text{Fresh weight} - \text{Dry weight}}{\text{Dry weight}} \times 100\%$$

142 Soil pH was measured using a pH meter (Mettler-Toledo FE28, Switzerland) after shaking the soil  
143 samples with deionized water at a 1:2.5 soil-to-water ratio. Soil organic carbon (SOC) concentration was  
144 determined by a CE400 elemental analyzer (Elementar vario ISOTOPE cube, Germany), after removing  
145 carbonates with 5% HCl. Soil samples for element analysis were digested with concentrated HNO<sub>3</sub>, HF,  
146 and HClO<sub>4</sub> (Bing et al., 2022). The concentrations of major elements (Al, Ba, Ca, Fe, K, Mg, Mn, Na, P,  
147 Sr, Ti, V, and Zn) in the digests were determined using an inductively coupled plasma atomic emission  
148 spectrometry (ICP-AES, Optima 2000, USA), and the concentrations of trace elements (Cd, Co, Cr, Cu,  
149 Mo, Ni, Pb, Sb, and Tl) were determined using an inductively coupled plasma mass spectrometry (ICP-  
150 MS, Agilent 7700x, USA), with SPEX™ serving as the standard solution. Quality control was ensured  
151 by analyzing replicates, blanks, and reference material (BW07405, China). The recovery of the reference  
152 material was routinely within the range of 95-105%, and the precision and accuracy of the analyses were

153 < 5% (relative standard deviation).

## 154 **2.4 Environmental data extraction and calculation**

155 The MAT and MAP in the study area were collected from the WorldClim database  
156 (<https://www.worldclim.org>) with a resolution of 1 km. The aridity index (AI), calculated as the ratio of  
157 MAP to potential evapotranspiration (PET), was sourced from the Global Drought Index and Potential  
158 Evapotranspiration Database provided by the Plant Data Center of Chinese Academy of Sciences  
159 ([doi.org/10.6084, CSTR:34735.11.PLANTDATA.0065](https://doi.org/10.6084, CSTR:34735.11.PLANTDATA.0065), Zomer et al., 2022). The normalized difference  
160 vegetation index (NDVI) from 2001 to 2015 was derived from the Advanced Very High-Resolution  
161 Radiometer (AVHRR) dataset developed by the Global Inventory Modeling and Mapping Studies  
162 (GIMMS) group (<https://ecocast.arc.nasa.gov/data/pub/gimms/3g.v1/>), with a resolution of 1/12°.  
163 Atmospheric N deposition across China (1980-2015) were derived from Yu et al. (2019). Parent rock  
164 data for the SOTER geological reservoir at a scale of 1: 1000000 in Chinese provinces (1990) were  
165 obtained from the National Earth System Science Data Center (<http://www.geodata.cn>). The soil type  
166 data were digitized from the 1:1000000 Soil Map compiled by the National Soil Census Office in 1995  
167 and obtained from the Resource and Environmental Science Data Center (<https://www.resdc.cn>).

168 The chemical index of alteration (CIA) was used to indicate the level of chemical weathering at  
169 each site (Nesbitt and Young, 1982).

$$170 \quad CIA = \frac{Al_2O_3}{(Al_2O_3 + Na_2O + K_2O + CaO^*)} \times 100$$

171 where the oxide is given in molar ratio. The CaO\* value represents the amount of CaO derived from  
172 silicate minerals and was corrected following the method proposed by McLennan (1993): when  $CaO \leq$   
173  $Na_2O$ , CaO\* is taken as the measured CaO content; when  $CaO > Na_2O$ , CaO\* is assumed to equal  $Na_2O$ .

## 174 **2.5 Statistical analysis**

175 All statistical analyses were conducted using R (version 4.3.1). To test differences in element  
176 concentrations among soil horizons, we employed linear mixed-effect models using the “lmer” function  
177 from the “lme4” package, where soil horizon was treated as a fixed factor and sampling site as a random  
178 factor. Regression analyses were conducted to examine the spatial distribution characteristics of each  
179 element. To explore the compositional differences in elemental assemblages across soil horizons and to  
180 assess the influence of environmental variables on soil element variation, redundancy analysis (RDA)

181 was conducted using the “rda” function in the “vegan” package. Correlation analyses were conducted  
182 separately for each soil horizon to identify horizon-specific relationships between elemental  
183 concentrations and environmental drivers. Furthermore, simple linear regression was employed to  
184 quantify the individual explanatory power ( $R^2$ ) of each environmental variable for each element. The  
185 cumulative explanatory power of all environmental factors was also calculated to evaluate their combined  
186 influence on element variation.

### 187 **3 Data description and evaluation**

188 This dataset provides a comprehensive and continental-scale characterization of soil element composition  
189 across China’s mountains, spanning five major climatic zones and three pedogenetically distinct soil  
190 horizons. The dataset includes quantitative measurements of 24 elements, thereby offering a holistic view  
191 of soil geochemistry in mountain regions. The dataset integrates information from extensive field surveys,  
192 laboratory analyses, high-resolution satellite-derived vegetation indices, and ancillary environmental  
193 data compiled from national and global databases. To ensure data consistency and comparability across  
194 sites, all soil samples were collected following standardized sampling protocols and analyzed using  
195 uniform laboratory procedures and instrumentation. In total, nine key environmental drivers were  
196 compiled and categorized into four groups, including climate variables (e.g., MAT, MAP, AI), vegetation  
197 characteristics (e.g., vegetation type, NDVI), basic soil properties (e.g., pH, moisture), and atmospheric  
198 nitrogen deposition levels. These integrated variables enable robust evaluation of the interactions  
199 between environmental factors and element distributions in soils.

#### 200 **3.1 Elemental concentrations across soil horizons**

201 Elemental concentrations in mountain soils exhibited a wide dynamic range, spanning over six orders of  
202 magnitude. The highest mean concentration was observed for SOC (127,699 mg/kg), while the lowest  
203 was for Tl (0.56 mg/kg, Fig. 2). The overall elemental mass ratio follows the pattern of  $C_{227038} : Al_{100998} :$   
204  $Fe_{46599} : K_{30204} : Ca_{19164} : Na_{14734} : Mg_{12201} : Ti_{5809} : P_{1373} : Mn_{1271} : Ba_{839} : Sr_{233} : Zn_{171} : V_{102} : Cr_{87.1} : Pb_{71.1} :$   
205  $Ni_{30.3} : Cu_{28.4} : Co_{13.2} : Be_{3.31} : Sb_{2.92} : Mo_{2.04} : Cd_{1.18} : Tl_1$ , underscoring the compositional diversity shaped  
206 by both natural and anthropogenic processes in mountainous environments.

207 Pronounced stratification of elemental concentrations was observed across the three soil horizons  
208 (Fig. 3). The O horizon, enriched in organic matter, exhibited significantly higher concentrations of major  
209 elements (e.g., carbon, Ca, and P), alongside elevated levels of several trace elements (e.g., Cd, Mn, Zn,



210 Pb, and Sb). This enrichment pattern is consistent with the accumulation of both biogenic nutrients and  
211 atmospherically deposited pollutants. In particular, the elevated concentrations of Cd, Pb, and Sb in the  
212 O horizon reflect anthropogenic inputs through long-range atmospheric transport and subsequent  
213 deposition (Bing et al., 2019, 2021). These findings reinforce the role of the O horizon as a critical  
214 biogeochemical interface where atmospheric inputs are retained and processed. In contrast, lithogenic  
215 elements such as Al, Fe, K, Na, Mg, Ti, Sr, and V showed increasing concentrations with depth,  
216 particularly in the A and C horizons (Fig. 3). This trend reflects the growing influence of parent material  
217 composition and geochemical weathering processes with depth, where the contributions from organic  
218 matter decline and pedogenic processes such as mineral dissolution and secondary mineral formation  
219 dominate (Agnan et al., 2019; Kirkby et al., 2018; Woodruff et al., 2009). The systematic increase in  
220 these elements suggests long-term pedogenic accumulation, consistent with the downward translocation  
221 of weathering minerals and reduced biological cycling in subsurface horizons. Overall, this vertical  
222 differentiation of elemental concentrations across soil horizons underscores the combined effects of  
223 biological activity, atmospheric deposition, and geochemical weathering in shaping the composition and  
224 distribution of soil elements in mountainous ecosystems.

### 225 **3.2 Spatial distribution of soil elements across China's mountains**

226 The spatial distribution of soil elements across China's mountains reveals complex patterns along  
227 latitudinal, longitudinal, and altitudinal gradients (Fig. 4), indicating the integrated influence of climatic,  
228 geological, and biological factors. Latitudinal trends in element concentrations were evident for several  
229 elements. Notably, concentrations of K, Mn, Mo, Ba, and Sr increased consistently with latitude,  
230 reflecting latitudinal variation in temperature-mediated weathering processes and element cycling  
231 (Moreno-Jiménez et al., 2022). In contrast, elements such as Ca, Mg, Na, Ni, Cu, Cd, Co, and Zn  
232 exhibited unimodal distribution patterns, with peak concentrations in mid-latitude regions, particularly  
233 at Mts. Suyukou, Wuyuezai, and Guandi. These non-linear patterns may arise from the combined  
234 influence of regional precipitation regimes, variable soil development stages, and differential  
235 atmospheric deposition (Bing et al., 2021; Luo et al., 2016a; Ren et al., 2019). Site-specific anomalies  
236 were also observed, indicating the strong influence of localized geological conditions. For instance, the  
237 high Ca concentrations at Mt. Gongga and elevated Ba and Sr concentrations at Mt. Dabie are attributed  
238 to distinctive lithological features and mineralogical compositions at these locations, which can override

239 broader climatic or biogeographical trends (Yang et al., 2015; Zhi et al., 2004).

240 Elemental distributions along the longitudinal gradient also exhibited significant patterns.  
241 Concentrations of Mn, Mo, and Zn increased from west to east across the study area, while Mg, Cr, and  
242 V showed declining trends in the same direction (Fig. 4). Phosphorus exhibited a non-monotonic  
243 longitudinal pattern, with concentrations decreasing initially and then increasing towards the eastern  
244 regions. These longitudinal patterns may reflect transitions in geologic substrates, soil parent materials,  
245 and regional differences in anthropogenic influence (Yang et al., 2022). Altitudinal variation in soil  
246 elemental concentrations further highlights the influence of mountain-specific environmental gradients.  
247 Concentrations of certain heavy metals (e.g., Cd, Cr, and V) increased significantly with altitude, while  
248 Cu and Ni exhibited unimodal distribution patterns (Fig. 4). These altitudinal patterns are likely shaped  
249 by altitude-driven shifts in local climatic conditions, vegetation type, and soil-forming processes, as well  
250 as differences in parent material exposure and erosion dynamics (Moreno-Jiménez et al., 2022; Yang et  
251 al., 2022).

### 252 **3.3 Environmental drivers of soil element composition**

253 The elemental composition of soils across China's mountains is significantly influenced by a combination  
254 of climatic, edaphic, and biogeographic factors. Statistical analyses revealed that variables such as MAT,  
255 MAP, AI, NDVI, CIA, soil pH, latitude, and soil moisture were significantly correlated with the  
256 concentrations of multiple elements ( $p < 0.05$ , Fig. 5). Climate- and vegetation-related variables showed  
257 negative correlations with SOC, P, Ca, Mg, Na, Mn, Ba, and Sr ( $p < 0.05$ ). These relationships suggest  
258 that cooler and drier sites, typically at higher altitudes or in arid regions, tend to accumulate higher  
259 concentrations of these elements, due to reduced microbial decomposition, slower organic matter  
260 turnover, and limited leaching under low-temperature and low-precipitation conditions (Moreno-Jiménez  
261 et al., 2019, 2023). Conversely, warmer and more vegetated environments may enhance biological  
262 cycling and leaching, leading to lower elemental retention in soils. Soil pH emerged as a key factor  
263 influencing elemental availability and retention. Most elements (except SOC, Fe, Sb, Pb, Tl, and Ti)  
264 exhibited positive correlations with pH (Fig. 5), indicating that higher pH conditions favor the retention  
265 or reduce mobility of these elements. This pattern reflects the well-established role of pH in controlling  
266 solubility, adsorption, and precipitation processes in the soil matrix (Barrow et al., 2023). Distinct vertical  
267 patterns in elemental composition were observed across soil horizons, reflecting the transition from

268 biologically active surface layers to more geochemically stable subsurface zones (Bing et al., 2021;  
269 Cronan et al., 2018; Jobbágy and Jackson, 2001). The O horizon exhibited elevated concentrations of  
270 SOC, P, Ca, Sr, and Cd, corresponding to inputs from plant litter, root exudates, and atmospheric  
271 deposition. The A horizon showed intermediate concentrations, indicating a mixing zone influenced by  
272 both surface biological activity and subsurface geochemical processes. The C horizon was enriched in  
273 lithogenic elements such as Ti, Al, Fe, and V, consistent with its proximity to parent material and  
274 dominance of mineral weathering processes.

275 The explanatory power of environmental drivers varied by both elements and horizons (Fig. 6). In  
276 the O horizon, climate and vegetation variables accounted for a substantial proportion of the variability  
277 in Al, Be, and Cd, indicating a high sensitivity of surface layers to environmental inputs. In the A horizon,  
278 the exceptionally high explanatory power observed for Fe (>200%) likely results from the combined  
279 effects of redox conditions, clay mineral formation, and complexation with organic matter (Dong et al.,  
280 2023), although this warrants further investigation. In the C horizon, Na exhibited relatively high  
281 explained variance, likely linked to its association with the weathering of Na-rich parent minerals. In  
282 contrast, elements such as Sb, Tl, and V consistently showed low explanatory power across all horizons,  
283 implying that their distributions are primarily controlled by lithological factors not captured by the  
284 environmental factors in this study. The influence of environmental factors on SOC and other biologically  
285 cycled elements decreased markedly with depth, consistent with the reduced biological activity and  
286 increasing geogenic control in subsurface horizons (Jobbágy and Jackson, 2001; Sayer et al., 2020). In  
287 contrast, pH and CIA became progressively more influential in the A and C horizons, highlighting the  
288 increasing importance of geochemical stabilization and mineral transformation processes with depth.

#### 289 **4 Potential applications of the dataset**

290 Soils are integral to global biogeochemical cycles, directly influencing ecosystem productivity, nutrient  
291 availability, and carbon storage. Understanding soil elemental composition and spatial variability is  
292 essential for assessing ecosystem function and predicting responses to environmental changes (Schimel  
293 et al., 2015). However, a persistent challenge in Earth system science has been the scarcity of high-  
294 resolution, field-validated dataset, particularly in mountain regions where complex topography, diverse  
295 vegetation, and steep climate gradients complicate both empirical and model-based analyses (Luo et al.,  
296 2016b; Tito et al., 2020; Todd-Brown et al., 2013). This comprehensive, multi-element soil dataset fills

297 a critical data gap by providing spatially explicit measurements of 24 elements across 30 mountain  
298 regions in China, spanning five major climatic zones and three soil development horizons. It offers unique  
299 opportunities for a wide range of applications in Earth system science.

300 *Advancing biogeochemical modeling.* The dataset is well-suited for parameterizing, calibrating, and  
301 validating a variety of biogeochemical models that simulate nutrient cycling, soil organic matter  
302 dynamics, and element transport under changing environmental conditions. For instance, decomposition  
303 models typically rely on the stoichiometry of carbon and nutrients, as well as interactions with  
304 environmental drivers such as temperature, moisture, and pH (Fang et al., 2019; Feng and Zhu, 2021).  
305 Our dataset provides detailed measurements of these variables across spatial and vertical gradients,  
306 enabling more accurate estimation of model parameters that govern decomposition rates, mineralization,  
307 and nutrient retention. The dataset also enables model validation through comparison between simulated  
308 outputs and observed element concentrations in diverse mountain ecosystems. **In addition, the inclusion**  
309 **of horizon-specific data (O, A, and C horizons), weathering indices, and lithological information provides**  
310 **valuable input for soil formation and rock weathering models. Process-based models like SoilGen or**  
311 **conceptual frameworks such as CLORPT (climate, organisms, relief, parent material, and time) can**  
312 **benefit from the dataset's vertical resolution and environmental coverage to simulate pedogenesis, profile**  
313 **evolution, and mineral nutrient release across climate gradients. Accordingly, the dataset can serve as a**  
314 **regional benchmark for calibrating and validating long-term soil development models, particularly in**  
315 **mountainous regions where such data are scarce yet critically needed.**

316 *Enhancing soil quality assessment and ecosystem risk evaluation.* Beyond modeling, the dataset  
317 provides a valuable reference for assessing soil quality and ecological risks in mountain regions.  
318 Measurements of SOC and macronutrient concentrations (e.g., P, K, and Ca) serve as indicators of soil  
319 fertility and ecosystem productivity (Bauters et al., 2022; Cunha et al., 2022; Rizzo et al., 2024).  
320 Simultaneously, the inclusion of micronutrients and trace elements enables evaluation of potential  
321 ecological hazards associated with heavy metal accumulation (Hou et al., 2025; Jin et al., 2024; Zhao et  
322 al., 2024). By capturing both beneficial and toxic elements, the dataset supports the identification of  
323 nutrient-deficient or polluted soils, informing the development of region-specific soil quality benchmarks.  
324 This is particularly relevant for mountainous ecosystems, where natural heterogeneity in soil properties  
325 can lead to localized environmental vulnerabilities. Furthermore, the dataset offers a foundation for

326 integrated assessments of soil health and ecosystem services, including nutrient cycling efficiency,  
327 pollutant buffering capacity, and biodiversity support.

328 *Supporting scenario analysis and climate adaptation planning.* By linking elemental concentrations  
329 with environmental drivers (e.g., climate variables, vegetation indices, and soil chemical properties), this  
330 dataset enables predictive analyses of how soil function may shift under future environmental conditions.  
331 For instance, projections of climate change, altered precipitation regimes, or land-use intensification can  
332 be used to model potential changes in soil nutrient availability, carbon storage, and heavy metal mobility  
333 (Giovannelli et al. 2023; Ochoa-Hueso et al., 2023). These capabilities are essential for developing  
334 adaptive land management strategies aimed at enhancing soil resilience and ecosystem sustainability in  
335 vulnerable mountain regions.

336 *Contributing to global soil and ecosystem monitoring initiatives.* The dataset contributes to global  
337 efforts in soil monitoring and environmental data sharing, such as those led by the Global Soil Partnership  
338 (GSP), the International Soil Reference and Information Centre (ISRIC), and global biogeochemical  
339 databases (e.g., SoilGrids, GEOTRACES) (Shi et al., 2025). Its high spatial resolution, standardized  
340 sampling protocols, and comprehensive coverage make it a valuable input for global-scale assessments  
341 of soil health, elemental cycling, and climate-soil-ecosystem interactions.

342 In summary, this dataset represents a significant advancement in the empirical foundation available  
343 for Earth system research in mountainous environments. It offers broad applicability for improving  
344 biogeochemical models, refining soil quality assessments, evaluating ecological risks, and informing  
345 sustainable land management and climate adaptation strategies. By enabling deeper understanding of soil  
346 processes across complex environmental gradients, this dataset contributes to ongoing efforts to conserve  
347 and manage mountain ecosystems in the face of accelerating global change.

## 348 **5 Data availability**

349 The database is freely accessible via the National Tibetan Plateau/Third Pole Environment Data Center  
350 at <https://doi.org/10.11888/Terre.tpd.302620> or <https://cstr.cn/18406.11.Terre.tpd.302620> (Wu et al.,  
351 2025b). The dataset provides comprehensive information for each sample, including mountain affiliation,  
352 geographical coordinates, climatic characteristics, vegetation type, soil type, parent rock type,  
353 normalized difference vegetation index, atmospheric nitrogen deposition rates, soil physicochemical  
354 properties, chemical weathering indices, and concentrations of 24 soil elements. The data are stored in

355 Excel spreadsheet format, accompanied by a separate data documentation file that describes variable  
356 names, units, and definitions.

### 357 **Author contributions**

358 BHJ, WuYH, and ZG designed the experiments. BHJ and LJ sampled the soils, BHJ, WangYH, YWZ,  
359 and ZJ performed the analysis of soil samples. WYY, BHJ, and WangYH analyzed the data. WYY and  
360 BHJ wrote the first draft of the manuscript. WYY, BHJ, WangYH, YWZ, ZJ, WuYH, LJ, and ZG revised  
361 and improved the manuscript. All authors read and approved the final manuscript.

### 362 **Competing interests**

363 The contact author has declared that none of the authors has any competing interests.

### 364 **Financial support**

365 This study was supported by the Science and Technology Projects of Xizang Autonomous Region, China  
366 (XZ202501ZY0054), Sichuan Science and Technology Program (2024ZYD0038), the Science and  
367 Technology Research Program of Institute of Mountain Hazards and Environment, Chinese Academy of  
368 Sciences (IMHE-ZDRW-06).

### 369 **References**

- 370 Agnan, Y., Courault, R., Alexis, M. A., Zanardo, T., Cohen, M., Sauvage, M., and Castrec-Rouelle, M.:  
371 Distribution of trace and major elements in subarctic ecosystem soils: Sources and influence of  
372 vegetation, *Sci. Total Environ.*, 682, 650-662. <https://doi.org/10.1016/j.scitotenv.2019.05.178>, 2019.
- 373 Antonelli, A., Kissling, W., Flantua, S. G., Bermúdez, M. A., Mulch, A., Muellner-Riehl, A. N., Kreft,  
374 H., Linder, H. P., Badgley, C., Fjeldså, J., Fritz, S. A., Rahbek, C., Herman, F., Hooghiemstra, H.,  
375 and Hoorn, C.: Geological and climatic influences on mountain biodiversity, *Nat. Geosci.*, 11, 718-  
376 725, <https://doi.org/10.1038/s41561-018-0236-z>, 2018.
- 377 Augusto, L., Achat, D. L., Jonard, M., Vidal, D., and Ringeval, B.: Soil parent material—A major driver  
378 of plant nutrient limitations in terrestrial ecosystems, *Global Change Biol.*, 23, 3808-3824,  
379 <https://doi.org/10.1111/gcb.13691>, 2017.
- 380 Barrow, N. J., and Hartemink, A. E.: The effects of pH on nutrient availability depend on both soils and  
381 plants, *Plant Soil*, 487, 21-37, <https://doi.org/10.1007/s11104-023-05960-5>, 2023.
- 382 Bauters, M., Janssens, I. A., Wasner, D., Doetterl, S., Vermeir, P., Griepentrog, M., Drake, T. W., Six, J.,  
383 Barthel, M., Baumgartner, S., Van Oost, K., Makelele, I. A., Ewango, C. E., Verheyen, K., and

384 Boeckx, P.: Increasing calcium scarcity along Afrotropical forest succession, *Nat. Ecol. Evol.*, 6,  
385 1122-1131, <https://doi.org/10.1038/s41559-022-01810-2>, 2022.

386 Bing, H. J., Qiu, S. J., Tian, X., Li, J., Zhu, H., Wu, Y. H., and Zhang, G.: Trace metal contamination in  
387 soils from mountain regions across China: Spatial distribution, sources, and potential drivers, *Soil*  
388 *Ecol. Lett.*, 3, 189-206, <https://doi.org/10.1007/s42832-021-0080-8>, 2021.

389 Bing, H. J., Liu, Y., Huang, J. C., Tian, X., Zhu, H., and Wu, Y. H.: Dam construction attenuates trace  
390 metal contamination in water through increased sedimentation in the Three Gorges Reservoir, *Water*  
391 *Res.*, 217, 118419, <https://doi.org/10.1016/j.watres.2022.118419>, 2022.

392 Bing, H. J., Wu, Y. H., Li, J., Xiang, Z. X., Luo, X. S., Zhou, J., Sun, H. Y., and Zhang, G.: Biomonitoring  
393 trace element contamination impacted by atmospheric deposition in China's remote mountains, *Atmos.*  
394 *Res.*, 224, 30-41, <https://doi.org/10.1016/j.atmosres.2019.03.018>, 2019.

395 Bing, H. J., Wu, Y. J., Zhou, J., Li, R., Luo, J., and Yu, D.: Vegetation and cold trapping modulating  
396 elevation-dependent distribution of trace metals in soils of a high mountain in Eastern Tibetan  
397 Plateau, *Sci. Rep.*, 6, 24081, <https://doi.org/10.1038/srep24081>, 2016.

398 Cronan, C. S.: Soil Biogeochemistry, In: *Ecosystem Biogeochemistry*, Springer Textbooks in Earth  
399 Sciences, Geography and Environment, Springer, Cham, 11-29, [https://doi.org/10.1007/978-3-319-](https://doi.org/10.1007/978-3-319-66444-6_2)  
400 [66444-6\\_2](https://doi.org/10.1007/978-3-319-66444-6_2), 2018.

401 Cui, Y. X., Bing, H. J., Moorhead, D. L., Delgado-Baquerizo, M., Ye, L. P., Yu, J. L., Zhang, S. P., Wang,  
402 X., Peng, S. S., Guo, X., Zhu, B., Chen, J., Tan, W. F., Wang, Y. Q., Zhang, X. C., and Fang, L. C.:  
403 Ecoenzymatic stoichiometry reveals widespread soil phosphorus limitation to microbial metabolism  
404 across Chinese forests, *Commun. Earth Environ.*, 3, 184, [https://doi.org/10.1038/s43247-022-](https://doi.org/10.1038/s43247-022-00523-5)  
405 [00523-5](https://doi.org/10.1038/s43247-022-00523-5), 2022.

406 Cunha, H. F., Andersen, K. M., Lugli, L. F., Santana, F. D., Aleixo, I. F., Moraes, A. M., Garcia, S., di  
407 Ponzio, R., Mendoza, E. O., Brum, B., Rosa, J. S., Cordeiro, A. L., Portela, B. T., Ribeiro, G., Coelho,  
408 S. D., de Souza, S. T., Silva, L. S., Antonieto, F., Pires, M. D., Salomão, A. C., Miron, A. C., de  
409 Assis, R. L., Domingues, T. F., Aragão, L. E., Meir, P., Camargo, J. L., Manzi, A. O., Nagy, L.,  
410 Mercado, L. M., Hartley, I. P., and Quesada, C. A.: Direct evidence for phosphorus limitation on  
411 Amazon forest productivity, *Nature*, 608, 558-562, <https://doi.org/10.1038/s41586-022-05085-2>,  
412 2022.

413 Dai, Z. M., Guo, X., Lin, J. H., Wang, X., He, D., Zeng, R. J., Meng, J., Luo, J. P., Delgado-Baquerizo,  
414 M., Moreno-Jiménez, E., Brookes, P.C., and Xu, J. M.: Metallic micronutrients are associated with  
415 the structure and function of the soil microbiome, *Nat. Commun.* 14, 8456,  
416 <https://doi.org/10.1038/s41467-023-44182-2>, 2023.

417 Dainese, M., Crepaz, H., Bottarin, R., Fontana, V., Guariento, E., Hilpold, A., Obojes, N., Paniccia, C.,  
418 Scotti, A., Seeber, J., Steinwandter, M., Tappeiner, U., and Niedrist, G.: Global change experiments  
419 in mountain ecosystems: A systematic review, *Ecol. Monogr.*, 94, e1632,  
420 <https://doi.org/10.1002/ecm.1632>, 2024.

421 Dong, H., Zeng, Q., Sheng, Y., Chen, C., Yu, G., and Kappler, A.: Coupled iron cycling and organic  
422 matter transformation across redox interfaces, *Nat. Rev. Earth Environ.*, 4, 659-673,  
423 <https://doi.org/10.1038/s43017-023-00470-5>, 2023.

424 Elser, J. J., Fagan, W. F., Kerkhoff, A. J., Swenson, N. G., and Enquist, B. J.: Biological stoichiometry of  
425 plant production: metabolism, scaling and ecological response to global change, *New Phytol.*, 186,  
426 593-608, <https://doi.org/10.1111/j.1469-8137.2010.03214.x>, 2010.

427 Fang, X. M., Zhang, X. L., Chen, F. S., Zong, Y. J., Bu, W. S., Wan, S. Z., Luo, Y. Q., and Wang, H. M.:  
428 Phosphorus addition alters the response of soil organic carbon decomposition to nitrogen deposition  
429 in a subtropical forest, *Soil Biol. Biochem.*, 133, 119-128,  
430 <https://doi.org/10.1016/j.soilbio.2019.03.005>, 2019.

431 Feng, J. G., and Zhu, B.: Global patterns and associated drivers of priming effect in response to nutrient  
432 addition, *Soil Biol. Biochem.*, 153, 108118, <https://doi.org/10.1016/j.soilbio.2020.108118>, 2021.

433 Feng, W., Mariotte, P., Gu, J., Song, X., Yang, J., Yang, F., Zhao, Y., and Zhang, G.: Impacts of geography,  
434 climate, soil properties and vegetation characteristics on soil C:N:P stoichiometry across the  
435 Qinghai-Tibetan Plateau, *Pedosphere*, <https://doi.org/10.1016/j.pedsph.2024.06.012>, 2024.

436 Fernández-Martínez, M.: From atoms to ecosystems: Elementome diversity meets ecosystem functioning,  
437 *New Phytol.*, 234: 35-42, <https://doi.org/10.1111/nph.17864>, 2021.

438 Giovannelli, D.: Trace metal availability and the evolution of biogeochemistry, *Nat. Rev. Earth Environ.*,  
439 4, 597-598, <https://doi.org/10.1038/s43017-023-00477-y>, 2023.

440 Haghverdi, K., and Kooch, Y.: Effects of diversity of tree species on nutrient cycling and soil-related  
441 processes, *Catena*, 178, 335-344, <https://doi.org/10.1016/j.catena.2019.03.041>, 2019.



442 Han W. X., Fang J. Y., Reich, P. B., Woodward, F. I., and Wang, Z. H.: Biogeography and variability of  
443 eleven mineral elements in plant leaves across gradients of climate, soil and plant functional type in  
444 China, *Ecol. Lett.*, 14, 788-796, <https://doi.org/10.1111/j.1461-0248.2011.01641.x>, 2011.

445 Hay Mele, B., Monticelli, M., Leone, S., Bastoni, D., Barosa, B., Cascone, M., Migliaccio, F.,  
446 Montemagno, F., Ricciardelli, A., Toniatti, L., Rotundi, A., Cordone, A., and Giovannelli, D.:  
447 Oxidoreductases and metal cofactors in the functioning of the earth, *Essays Biochem.*, 67, 653-670,  
448 <https://doi.org/10.1042/EBC20230012>, 2023.

449 Hou, D. Y., Jia, X. Y., Wang, L. W., McGrath, S. P., Zhu, Y. G., Hu, Q., Zhao, F. J., Bank, M. S., O'Connor,  
450 D., and Nriagu, J.: Global soil pollution by toxic metals threatens agriculture and human health,  
451 *Science*, 388(6744), 316-321, <https://doi.org/10.1126/science.adr5214>, 2025.

452 IPCC: Climate Change 2021: The Physical Science Basis. Cambridge University Press, Cambridge, UK,  
453 2021.

454 Jin, J. Y., Zhao, D. Y., Wang, J. P., Wang, Y. H., Zhu, H., Wu, Y. H., Fang, L. C., and Bing, H. J.: Fungal  
455 community determines soil multifunctionality during vegetation restoration in metallic tailing  
456 reservoir, *J. Hazard Mater.*, 478, 135438, <https://doi.org/10.1016/j.jhazmat.2024.135438>, 2024.

457 Jobbágy, E. G., and Jackson, R. B.: The distribution of soil nutrients with depth: Global patterns and the  
458 imprint of plants, *Biogeochemistry*, 53, 51-77, <https://doi.org/10.1023/A:1010760720215>, 2001.

459 Jobbágy, E. G., and Jackson, R. B.: The uplift of soil nutrients by plants: Biogeochemical consequences  
460 across scales, *Ecology*, 85, 2380-2389, <https://doi.org/10.1890/03-0245>, 2004.

461 Kaspari, M. and Powers, J. S.: Biogeochemistry and geographical ecology: Embracing all twenty-five  
462 elements required to build organisms, *Am. Nat.*, 188, 62-73, <https://doi.org/10.1086/687576>, 2016.

463 Kirkby, M. J.: A conceptual model for physical and chemical soil profile evolution, *Geoderma*, 331, 121-  
464 130, <https://doi.org/10.1016/j.geoderma.2018.06.009>, 2018.

465 Kou, Y. P., Zhao, W. Q., Liu, Y. J., Wu, Y. H., Xiao, J. T., Wang, X. H., Bing, H. J., and Liu, Q.: Diversity  
466 patterns and drivers of methanotrophic gene distributions in forest soils across a large latitudinal  
467 gradient, *Glob. Ecol. Biogeogr.*, 30, 2004-2015, <https://doi.org/10.1111/geb.13362>, 2021.

468 Lu, L. M., Mao, L. F., Yang, T., Ye, J. F., Liu, B., Li, H. L., Sun, M., Miller, J. T., Mathews, S., Hu, H.  
469 H., Niu, Y. T., Peng, D. X., Chen, Y. H., Smith, S. A., Chen, M., Xiang, K. L., Le, C. T., Dang, V.  
470 C., Lu, A. M., Soltis, P. S., Soltis, D. E., Li, J. H., and Chen, Z. D.: Evolutionary history of the

471 angiosperm flora of China, *Nature*, 554, 234-238, <https://doi.org/10.1038/nature25485>, 2018.

472 Luo, W., Sardans, J., Dijkstra, F. A., Peñuelas, J., Lü, X. T., Wu, H., Li, M. H., Bai, E., Wang, Z., Han,  
473 X. and Jiang, Y.: Thresholds in decoupled soil-plant elements under changing climatic conditions,  
474 *Plant Soil*, 409, 159-173, <https://doi.org/10.1007/s11104-016-2955-5>, 2016a.

475 Luo, Y., Ahlström, A., Allison, S., Batjes, N., Brovkin, V., Carvalhais, N., Chappell, A., Ciais, P.,  
476 Davidson, E., Finzi, A., Georgiou, K., Guenet, B., Hararuk, O., Harden, J., He, Y., Hopkins, F., Jiang,  
477 L., Koven, C., Jackson, R., Jones, C. D., Lara, M. J., Liang, J., McGuire, A. D., Parton, W., Peng,  
478 C., Randerson, J. T., Salazar, A., Sierra, C. A., Smith, M. J., Tian, H., Todd-Brown, K. E. O., Torn,  
479 M., van Groenigen, K. J., Wang, Y. P., West, T. O., Wei, Y., Wieder, W. R., Xia, J., Xu, X., Xu, X.  
480 F., Zhou, T.: Toward more realistic projections of soil carbon dynamics by Earth system models,  
481 *Global Biogeochem. Cy.*, 30, 40-56, <https://doi.org/10.1002/2015GB005239>, 2016b.

482 Lynch, J. P., and St. Clair, S. B.: Mineral stress: The missing link in understanding how global climate  
483 change will affect plants in real world soils, *Field Crops Res.*, 90, 101-115,  
484 <https://doi.org/10.1016/j.fcr.2004.07.008>, 2004.

485 Maynard, D. G., and Curran, M. P.: Bulk density measurement in forest soils, *Soil sampling and methods*  
486 *of analysis*, 863-869, <https://doi.org/10.1201/978142000527>, 2007.

487 McLennan, S. M.: Weathering and Global Denudation, *J. Geol.*, 101, 295-303,  
488 <https://doi.org/10.1086/648222>, 1993.

489 Molina, A., Vanacker, V., Chadwick, O., Zhiminaicela, S., Corre, M. D., and Veldkamp, E.: Vegetation  
490 patterns associated with nutrient availability and supply in high-elevation tropical Andean  
491 ecosystems, *Biogeosciences*, 21, 3075-3091, <https://doi.org/10.5194/bg-21-3075-2024>, 2024.

492 Moreno-Jiménez, E., Maestre, F. T., Flagmeier, M., Guirado, E., Berdugo, M., Bastida, F., Dacal, M.,  
493 Díaz-Martínez, P., Ochoa-Hueso, R., Plaza, C., Rillig, M. C., Crowther, T. W., and Delgado-  
494 Baquerizo, M.: Soils in warmer and less developed countries have less micronutrients globally, *Glob.*  
495 *Change Biol.*, 29, 522-532, <https://doi.org/10.1111/gcb.16478>, 2022.

496 Moreno-Jiménez, E., Plaza, C., Saiz, H., Manzano, R., Flagmeier, M., and Maestre, F. T.: Aridity and  
497 reduced soil micronutrient availability in global drylands, *Nat. Sustain.*, 2, 371-377,  
498 <https://doi.org/10.1038/s41893-019-0262-x>, 2019.

499 Nagajyoti, P. C., Lee, K. D. and Sreekanth, T. V. M.: Heavy metals, occurrence and toxicity for plants: A

500 review, *Environ. Chem. Lett.*, 8, 199-216, <https://doi.org/10.1007/s10311-010-0297-8>, 2010.

501 Nesbitt, H. W., and Young, G. M.: Early Proterozoic climates and plate motions inferred from major  
502 element chemistry of lutites, *Nature*, 299, 715-717, <https://doi.org/10.1038/299715a0>, 1982.

503 Nogués-Bravo, D., Araújo, M. B., Errea, M. P., and Martínez-Rica, J. P.: Exposure of global mountain  
504 systems to climate warming during the 21st Century, *Global Environ. Chang.*, 17, 420-428,  
505 <https://doi.org/10.1016/j.gloenvcha.2006.11.007>, 2007.

506 Ochoa-Hueso, R., Delgado-Baquerizo, M., Risch, A. C., Ashton, L., Augustine, D., Bélanger, N.,  
507 Bridgham, S., Britton, A. J., Bruckman, V. J., Camarero, J. J., Cornelissen, G., Crawford, J. A.,  
508 Dijkstra, F. A., Diochon, A., Earl, S., Edgerley, J., Epstein, H., Felton, A., Fortier, J., Gagnon, D.,  
509 Greer, K., Griffiths, H. M., Halde, C., Hanslin, H. M., Harris, L. I., Hartsock, J. A., Hendrickson, P.,  
510 Hovstad, K. A., Hu, J., Jani, A. D., Kent, K., Kerdraon-Byrne, D., Khalsa, S. D. S., Lai, D. Y. F.,  
511 Lambert, F., LaMontagne, J. M., Lavergne, S., Lawrence, B. A., Littke, K., Leeper, A. C., Licht, M.  
512 A., Liebig, M. A., Lynn, J. S., Maclean, J. E., Martinsen, V., McDaniel, M. D., McIntosh, A. C. S.,  
513 Miesel, J. R., Miller, J., Mulvaney, M. J., Moreno, G., Newstead, L., Pakeman, R. J., Pergl, J., Pinno,  
514 B. D., Piñeiro, J., Quigley, K., Radtke, T. M., Reed, P., Rolo, V., Rudgers, J., Rutherford, P. M.,  
515 Sayer, E. J., Serrano-Grijalva, L., Strack, M., Sukdeo, N., Taylor, A. F. S., Truax, B., Tsuji, L. J. S.,  
516 van, G., Vaness, B. M., Van, S., Vítková, M., Weigel, R., Wilton, M. J., Yano, Y., Teen, E., and  
517 Bremer, E.: Bioavailability of macro and micronutrients across global topsoils: Main drivers and  
518 global change impacts, *Global Biogeochem. Cy.*, 37, e2022GB007680,  
519 <https://doi.org/10.1029/2022GB007680>, 2023.

520 Peñuelas, J., Fernández-Martínez, M., Ciais, P., Jou, D., Piao, S. L., Obersteiner, M., Vicca, S., Janssens,  
521 I. A., and Sardans, J.: The bioelements, the elementome, and the biogeochemical niche, *Ecology*,  
522 100, e02652, <https://doi.org/10.1002/ecy.2652>, 2019.

523 Ren, H., Zhou, Q., He, J., Hou, Y., Jiang, Y., Rodrigues, J. L. M., Cobb, A. B., Wilson, G. W. T., Hu, J.,  
524 and Zhang, Y.: Determining landscape-level drivers of variability for over fifty soil chemical  
525 elements, *Sci. Total Environ.*, 657, 279-286, <https://doi.org/10.1016/j.scitotenv.2018.12.024>, 2019.

526 Rizzo, G., Agus, F., Susanti, Z., Buresh, R., Cassman, K. G., Dobermann, A., Agustiani, N., Aristya, V.  
527 E., Batubara, S. F., Istiqomah, N., Oberthür, T., Pasuquin, J. M., Samijan, Witt, C., and Grassini, P.:  
528 Potassium limits productivity in intensive cereal cropping systems in Southeast Asia, *Nat. Food* 5,  
19

529 929-938, <https://doi.org/10.1038/s43016-024-01065-z>, 2024.

530 Sayer, E. J., Rodtassana, C., Sheldrake, M., Sheldrake, M., Bréchet, L. M., Ashford, O. S., Lopez-Sangil,  
531 L., Kerdraon-Byrne, D., Castro, B., Turner, B. L., Wright, S. J., and Tanner, E. V.: Revisiting nutrient  
532 cycling by litterfall -- Insights from 15 years of litter manipulation in old-growth lowland tropical  
533 forest, *Adv. Ecol. Res.*, 62, 173-223, <https://doi.org/10.1016/bs.aecr.2020.01.002>, 2020.

534 Schimel, D. S., Pavlick, R. P., Fisher, J. B., Asner, G. P., Saatchi, S. S., Townsend, P. A., Miller, C. E.,  
535 Frankenberg, C., Hibbard, K. A., and Cox, P. M.: Observing terrestrial ecosystems and the carbon  
536 cycle from space, *Global Change Biol.*, 21(5), 1762-1776, <https://doi.org/10.1111/gcb.12822>, 2015.

537 Shafiee, R. T., Diver, P., Snow, J. T., Zhang, Q., and Rickaby, R. E.: Marine ammonia-oxidising archaea  
538 and bacteria occupy distinct iron and copper niches, *ISME Commun.*, 1,  
539 <https://doi.org/10.1038/s43705-021-00001-7>, 2021.

540 Shangguan, W., Dai, Y., Duan, Q., Liu, B., and Yuan, H.: A global soil data set for Earth system modeling,  
541 *J. Adv. Model. Earth Syst.*, 6(1), 249-263, <https://doi.org/10.1002/2013MS000293>, 2014.

542 Shi, G. S., Sun, W. Y., Wei, S. G., Wei, Z. W., Yuan, H., Li, L., Sun, X. L., Zhang, Y. Liang, H. B., Li, D.  
543 X., Huang, F. N., Li, Q. L., Dai, Y. J.: A China dataset of soil properties for land surface modeling  
544 (version 2), *Earth Syst. Sci. Data*, 17, 517-543, <https://doi.org/10.5194/essd-17-517-2025>, 2025.

545 Steinnes, E., and Lierhagen, S.: Geographical distribution of trace elements in natural surface soils:  
546 Atmospheric influence from natural and anthropogenic sources, *Appl. Geochem.*, 88, 2-9,  
547 <https://doi.org/10.1016/j.apgeochem.2017.03.013>, 2018.

548 Sundqvist, M. K., Sanders, N. J. and Wardle, D. A.: Community and ecosystem responses to elevational  
549 gradients: processes, mechanisms and insights for global change, *Annu. Rev. Ecol. Evol. S.*, 44,  
550 261-280, <https://doi.org/10.1146/annurev-ecolsys-110512-135750>, 2013.

551 Tian, D., Reich, P. B., Chen, H. Y. H., Xiang, Y., Luo, Y., Shen, Y., Meng, C., Han, W., and Niu, S.: Global  
552 changes alter plant multi-element stoichiometric coupling, *New Phytol.*, 221(2), 807-817,  
553 <https://doi.org/10.1111/nph.15428>, 2019.

554 Tito, R., Vasconcelos, H. L., and Feeley, K. J.: Mountain ecosystems as natural laboratories for climate  
555 change experiments, *Front. For. Glob. Change*, 3, <https://doi.org/10.3389/ffgc.2020.00038>, 2020.

556 Todd-Brown, K. E., Randerson, J. T., Post, W. M., Hoffman, F. M., Tarnócai, C., Schuur, E. A., and  
557 Allison, S. D.: Causes of variation in soil carbon simulations from CMIP5 Earth system models and

558 comparison with observations, *Biogeosciences*, 10, 1717-1736, [https://doi.org/10.5194/bg-10-](https://doi.org/10.5194/bg-10-1717-2013)  
559 [1717-2013](https://doi.org/10.5194/bg-10-1717-2013), 2013.

560 Vallicrosa, H.: Beyond nitrogen and phosphorus, *Nat. Ecol. Evol.*, 6, 1056-1057,  
561 <https://doi.org/10.1038/s41559-022-01788-x>, 2022.

562 Wang, J., Hu, A., Meng, F., Zhao, W., Yang, Y., Soininen, J., Shen, J., and Zhou, J.: Embracing mountain  
563 microbiome and ecosystem functions under global change, *New Phytol.*, 234, 1987-2002,  
564 <https://doi.org/10.1111/nph.18051>, 2022.

565 Wang, Y., Bing, H., Moorhead, D. L., Hou, E., Wu, Y., Wang, J., Duan, C., Cui, Q., Zhang, Z., and Zhu,  
566 H.: Bacterial community structure modulates soil phosphorus turnover at early stages of primary  
567 succession, *Global Biogeochem. Cy.*, 38, e2024GB008174, <https://doi.org/10.1029/2024GB008174>,  
568 2024.

569 Woodruff, L. G., Cannon, W. F., Eberl, D. D., Smith, D. B., Kilburn, J. E., Horton, J. D., Garrett, R. G.,  
570 and Klassen, R. A.: Continental-scale patterns in soil geochemistry and mineralogy: Results from  
571 two transects across the United States and Canada, *Appl. Geochem.*, 24, 1369-1381,  
572 <https://doi.org/10.1016/j.apgeochem.2009.04.009>, 2009.

573 Wu, Y. Y., Wang, Y. H., Ochoa-Hueso, R., Hou, E. Q., Li, J., Zhu, H., Sardans, J., Fang, L. C., Wu, Y. H.,  
574 Zhang, G., Peñuelas, J., and Bing, H. J.: From bedrock to life activity and atmospheric deposition:  
575 Drivers of soil element coupling across horizons, *Environ. Res.*, 271, 121070,  
576 <https://doi.org/10.1016/j.envres.2025.121070>, 2025a.

577 Wu, Y. Y., Bing, H. J., Wang, Y. H., Yang, W. Z., Zhang, J., Wu, Y. H., Li, J., and Zhang, G.: Multi-  
578 element dataset across diverse climatic zones and soil profiles in China's mountains, National  
579 Tibetan Plateau/Third Pole Environment Data Center, <https://doi.org/10.11888/Terre.tpd.c.302620>,  
580 2025b.

581 Yang, W. Z., Bing, H. J., Tian, X., Liu, Y., Zhu, H., Fang, L. C., and Wu, Y. H.: Unearthing the importance  
582 of soil development in total phosphorus distribution in China's mountains, *Catena*, 228, 107193,  
583 <https://doi.org/10.2139/ssrn.4357696>, 2023.

584 Yang, Z. J., Bing, H. J., Zhou, J., Wu, Y. H., Sun, H. Y., Luo, J., Sun, S. Q., and Wang, J. P.: Variation of  
585 mineral composition along the soil chronosequence at the Hailuoguo Glacier foreland of Gongga  
586 Mountain, *Acta Pedol. Sin.*, 52, 507-516, <https://doi.org/10.11766/trxb201406180301>, 2015.

587 Yu, G. R., Jia, Y. L., He, N. P., Zhu, J. X., Chen, Z., Wang, Q. F., Piao, S. L., Liu, X. J., He, H. L., Guo,  
588 X. B., Wen, Z., Li, P., Ding, G. A., and Goulding, K.: Stabilization of atmospheric nitrogen  
589 deposition in China over the past decade, *Nat. Geosci.*, 12, 424-429, [https://doi.org/10.1038/s41561-](https://doi.org/10.1038/s41561-019-0352-4)  
590 [019-0352-4](https://doi.org/10.1038/s41561-019-0352-4), 2019.

591 Zhao, D., Bol, R., Wang, J., Jin, J., Wang, Y., Wang, T., Zhu, H., Wu, Y., Fang, L., and Bing, H.: Soil  
592 heavy metal pollution promotes extracellular enzyme production by mediating microbial  
593 community structure during vegetation restoration of metallic tailing reservoir, *Sci. Total Environ.*,  
594 948, 174783, <https://doi.org/10.1016/j.scitotenv.2024.174783>, 2024.

595 Zhao, W. Q., Kou, Y. P., Wang, X. H., Wu, Y. H., Bing, H. J., and Liu, Q.: Broad-scale distribution of  
596 diazotrophic communities is driven more by aridity index and temperature than by soil properties  
597 across various forests, *Glob. Ecol. Biogeogr.*, 29, 2119-2130, <https://doi.org/10.1111/geb.13178>,  
598 2020.s

599 Zhi, X. C., Jin, Y. B., Meng, Q., and Gao, T. S.: Trace element geochemistry of Raobazhai ultramafic  
600 complex, North Dabie Mountain, *Acta Petrol. Sin.*, 20, 463-472, 2004.

601 Zomer, R. J., Xu, J., and Trabucco, A.: Version 3 of the global aridity index and potential  
602 evapotranspiration database, *Sci. Data*, 9, 409, <https://doi.org/10.1038/s41597-022-01493-1>, 2022.

603 Zuo, Z. J., Reich, P. B., Qiao, X. J., Zhao, H. C., Zhang, L. J., Yang, L., Lv, T., Tang, Z. Y., Yu, D., and  
604 Wang, Z.: Coordination between bioelements induce more stable macroelements than  
605 microelements in wetland plants. *Ecol. Lett.*, 27, e70025, <https://doi.org/10.1111/ele.70025>, 2024.

606 **Figure legends**

607 **Fig. 1** Geographic distribution of the 30 China's mountains. AL, Mt. Ailao; AS, Mt. Ao; BCW, Mt.  
608 Baicaowa; CB, Mt. Changbai; DB, Mt. Dabie; DH, Mt. Dinghu; DX, Mt. Daxinganling; DYS, Mt.  
609 Daiyun; FJS, Mt. Fanjing; GD, Mt. Guandi; GGS, Mt. Gongga; HS, Mt. Han; JF, Mt. Jifeng; JG, Mt.  
610 Jiugong; JGS, Mt. Jinggang; LJ, Mt. Luoji; LG, Mt. Leigong; LJ, Mt. Luoji; ME, Mt. Maoer; NL, Mt.  
611 Nanling; QF, Mt. Qingfengxia; QL, Mt. Qinling; SHB, Mt. Saihanba; SN, Mt. Shennongjia; SWDS, Mt.  
612 Shiwandashan; SYK, Mt. Suyukou; TM, Mt. Tianmu; WGS, Mt. Wugong; WYZ, Mt. Wuyuezhai; WZS,  
613 Mt. Wuzhi; XX, Mt. Xiaoxinganling.

614 **Fig. 2** Frequency distribution of soil elements across the China's mountains. Red curve on each histogram  
615 represents the fitted normal distribution. The statistical parameters of the corresponding element are  
616 annotated in the upper left of each sub-figure.

617 **Fig. 3** Mean concentrations of 24 elements across different soil horizons. Lowercase letters indicate  
618 significant differences in each element among soil horizons ( $p < 0.05$ ), and error bars represent the  
619 standard error.

620 **Fig. 4** Spatial distribution of soil element concentrations across latitude, longitude, and altitude. The  
621 colors of the dots represent different soil horizons. Solid red lines represent the fitting relationships of  
622 elemental concentrations with latitude, longitude, and altitude ( $p < 0.05$ ).  $R^2$  less than 0.05 are not shown.

623 **Fig. 5** The environmental factors influencing the elemental concentrations in the soils. (a) Redundancy  
624 analysis (RDA) shows the relationships of soil elements with environmental factors across soil horizons.  
625 The inserted figure shows the distribution of samples along the axes. (b) Correlation heatmap shows the  
626 correlation between soil element concentrations and environmental variables in each soil horizon. The  
627 color and circle size represent the correlation coefficient, and \* indicates statistical significance ( $p < 0.05$ ).

628 SOC, soil organic carbon; MAP, mean annual precipitation; MAT, mean annual temperature; AI, aridity  
629 index; DIN, dissolved inorganic nitrogen; NDVI, normalized difference vegetation index; BD, bulk  
630 density; CIA, chemical index of alteration

631 **Fig. 6** Explanation of elemental variation by environmental factors based on regression modelling.  
632 Columns with different colors represent different environmental variables. Total height of each bar  
633 indicates the cumulative explanatory power. MAP, mean annual precipitation; MAT, mean annual  
634 temperature; AI, aridity index; DIN, dissolved inorganic nitrogen; NDVI, normalized difference

635 vegetation index; CIA, chemical index of alteration



**Table1** The basic information across China's mountains (n =30)

Climatic zone	Mountain ID	n	Latitude (°N)	Longitude (°E)	Altitude (m)	MAP (mm)	MAT (°C)	Vegetation types
Cold-temperate	DX	133	49.25-53.45	122.34-124.28	360-1370	514	-3.1	Broadleaf forest, Coniferous-broadleaf mixed forest, Coniferous forest
	BCW	36	40.82-40.83	117.60-117.61	1120-1710	539	6.0	Coniferous forest
	CB	58	42.06-42.30	127.83-128.13	1025-2000	828	-1.0	Broadleaf forest, Coniferous forest
	HS	51	44.19-44.27	118.41-118.72	1100-1400	400	1.0	Broadleaf forest, Coniferous-broadleaf mixed forest, Coniferous forest
Temperate	ME	12	45.39-45.39	127.68-127.68	400-400	599	2.7	Coniferous-broadleaf mixed forest
	SHB	36	42.33-42.47	117.29-117.51	1560-1870	452	1.0	Broadleaf forest, Coniferous-broadleaf mixed forest
	SYK	27	38.73-38.75	105.91-105.92	2030-2350	243	4.3	Coniferous forest
	XX	78	46.63-48.85	128.47-129.65	240-1420	639	0.2	Broadleaf forest, Coniferous-broadleaf mixed forest
	AS	84	33.79-33.96	107.30-107.50	1260-3150	786	6.2	Broadleaf forest, Coniferous-broadleaf mixed forest, Coniferous forest
	GD	42	37.89-37.90	111.43-111.44	1310-2200	5211	2.4	Broadleaf forest, Coniferous-broadleaf mixed forest, Coniferous forest, Shrub
Warm-temperate	JF	18	33.68-33.69	105.68-105.68	1785-1900	670	12.2	Coniferous forest Broadleaf forest,
	QF	27	34.00-34.04	107.44-107.44	1530-2100	737	7.6	Coniferous-broadleaf mixed forest Broadleaf forest,
	QL	66	34.02-34.16	107.61-107.80	870-2350	750	6.4	Coniferous-broadleaf mixed forest, Coniferous forest
	WYZ	42	38.72-38.73	113.84-113.86	1210-1880	476	6.9	Broadleaf forest, Coniferous-broadleaf mixed forest,

									Coniferous forest, Shrub
									Broadleaf forest,
	AL	45	24.50-24.54	100.99-101.03	2190-2655	971	14.1	Coniferous-broadleaf mixed forest	Coniferous-broadleaf mixed forest
	DB	45	31.09-31.10	115.77-115.81	400-1630	1562	11.4	Coniferous forest	Coniferous forest
	DH	27	23.17-23.18	112.52-112.54	210-586	1788	21.1	Coniferous-broadleaf mixed forest	Coniferous-broadleaf mixed forest
	DYS	30	25.64-25.65	118.22-118.22	1100-1510	1546	15.9	Coniferous-broadleaf mixed forest,	Coniferous forest
	FJS	19	27.90-27.91	108.70-108.72	1482-2095	1346	11.6	Broadleaf forest	Broadleaf forest,
	GGs	66	29.54-29.60	101.96-102.07	2000-4225	967	6.6	Coniferous forest, Shrub	Coniferous-broadleaf mixed forest,
	JG	27	29.38-29.40	114.58-114.62	580-1230	1635	13.8	Coniferous forest	Coniferous forest
Subtropical	JGS	30	26.51-26.63	114.11-114.17	925-1350	1727	14.0	Coniferous-broadleaf mixed forest	Coniferous-broadleaf mixed forest
	LG	24	26.36-26.38	108.16-108.21	1223-2155	1294	12.6	Broadleaf forest, Coniferous forest, Shrub	Broadleaf forest, Coniferous forest
	LJ	51	27.57-27.58	102.37-102.42	2200-3830	940	7.5	Broadleaf forest, Coniferous forest	Broadleaf forest, Coniferous forest
	NL	18	24.90-24.95	112.99-113.05	800-1545	1700	14.9	Coniferous-broadleaf mixed forest,	Coniferous-broadleaf mixed forest,
	SN	105	31.36-31.76	110.15-110.55	1110-3090	1274	7.7	Coniferous forest Broadleaf forest,	Coniferous forest Broadleaf forest,
	SWDS	45	21.88-21.90	107.90-107.92	393-708	1908	20.0	Coniferous-broadleaf mixed forest	Coniferous-broadleaf mixed forest
	TM	21	30.36-30.58	119.43-119.73	790-1460	1382	14.0	Coniferous-broadleaf mixed forest	Coniferous-broadleaf mixed forest
	WGS	27	27.46-27.46	114.16-114.17	778-1175	1767	13.6	Broadleaf forest	Broadleaf forest
Tropical	WZS	24	18.89-18.90	109.69-109.71	862-1818	1694	20.8	Broadleaf forest	Broadleaf forest

637 AL, Mt. Ailao; AS, Mt. Ao; BCW, Mt. Baicaowa; CB, Mt. Changbai; DB, Mt. Dabie; DH, Mt.

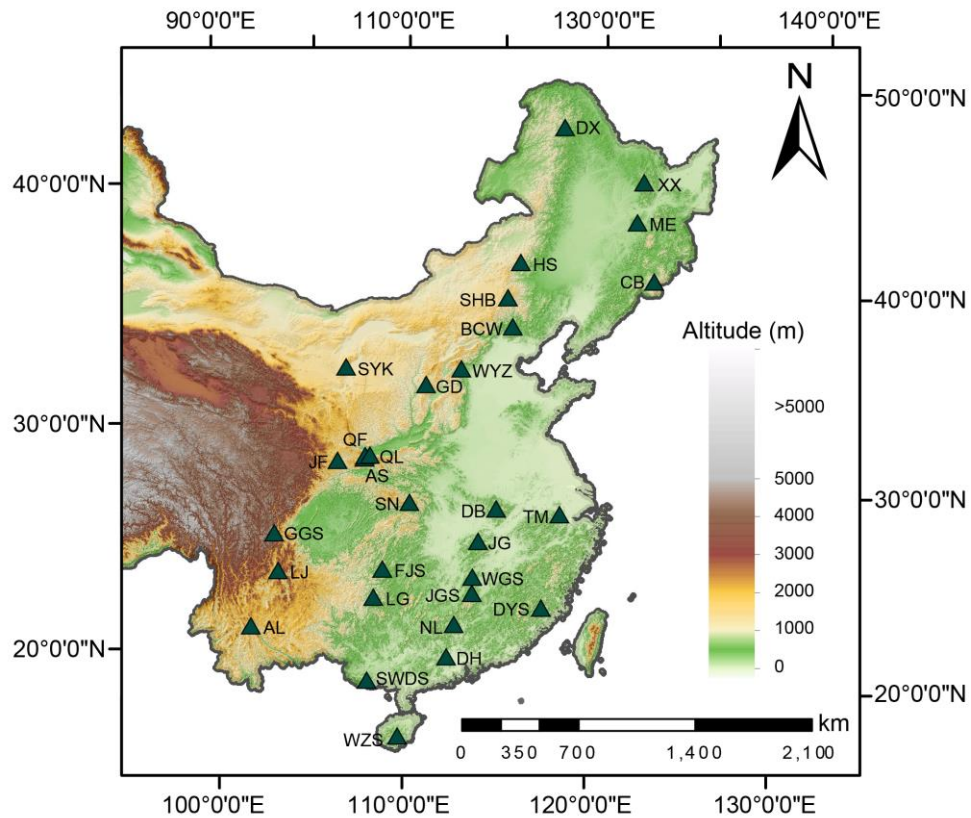
638 Dinghu; DX, Mt. Daxinganling; DYS, Mt. Daiyun; FJS, Mt. Fanjing; GD, Mt. Guandi; GGS, Mt.  
639 Gongga; HS, Mt. Han; JF, Mt. Jifeng; JG, Mt. Jiugong; JGS, Mt. Jinggang; LJ, Mt. Luoji; LG, Mt.  
640 Leigong; LJ, Mt. Luoji; ME, Mt. Maoer; NL, Mt. Nanling; QF, Mt. Qingfengxia; QL, Mt. Qinling;  
641 SHB, Mt. Saihanba; SN, Mt. Shennongjia; SWDS, Mt. Shiwandashan; SYK, Mt. Suyukou; TM, Mt.  
642 Tianmu; WGS, Mt. Wugong; WYZ, Mt. Wuyuezhai; WZS, Mt. Wuzhi; XX, Mt. Xiaoxinganling;  
643 MAP, mean annual precipitation; MAT, mean annual temperature.

**Table 2** The basic soil properties across the mountains (n =30)

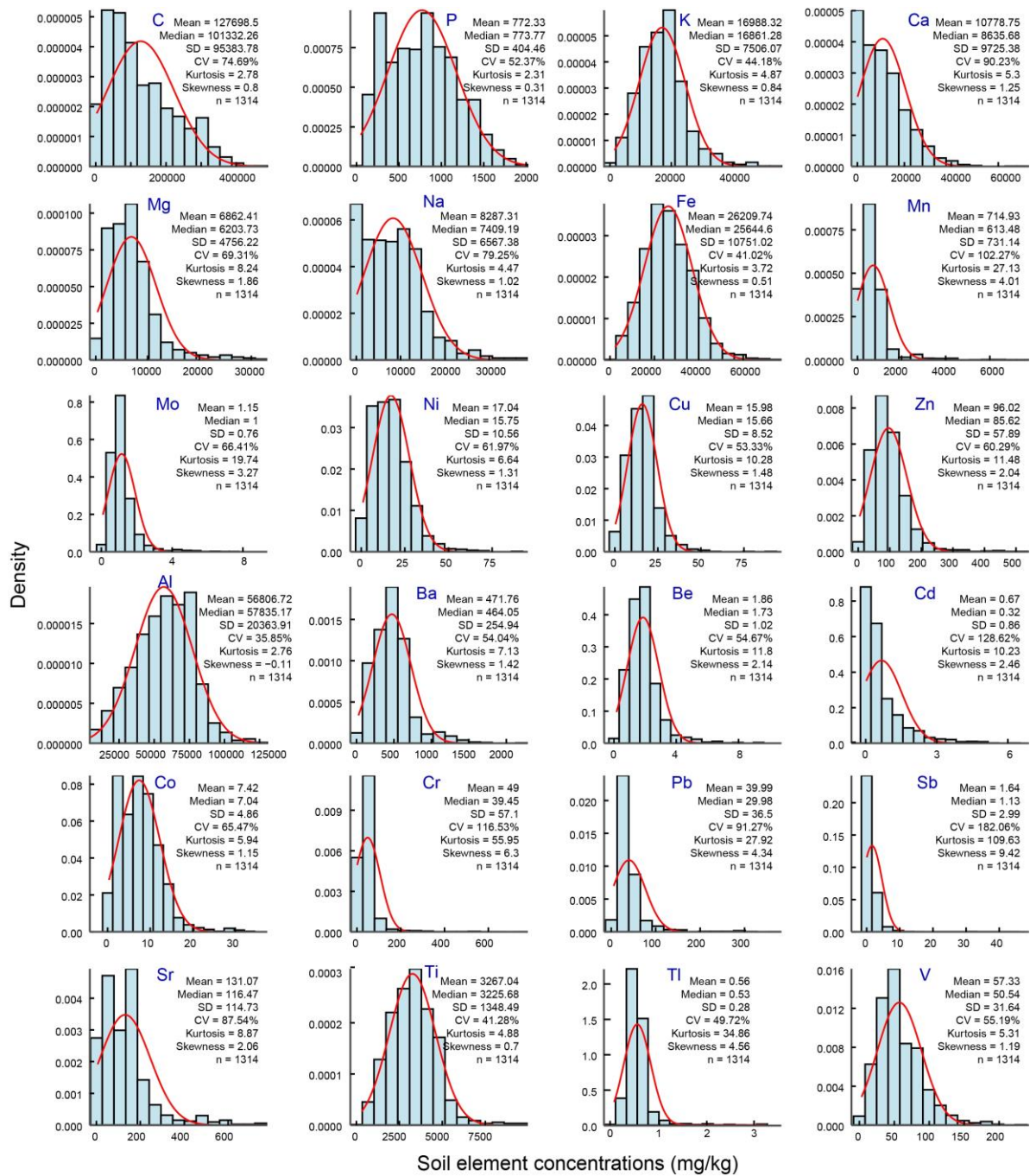
Climatic zone	Mountain ID	Horizon	BD (g/cm <sup>3</sup> )	Moisture (%)	pH	CIA
Cold-temperate	DX	O	0.11-0.21	70.0-182.2	3.37-6.73	53.40-67.58
		A	0.19-0.70	14.6-118.9	3.10-6.47	57.73-74.10
		C	0.50-1.39	9.1-44.6	3.70-6.44	57.6-74.04
	BCW	O	0.16-0.22	27.3-63.2	4.34-6.66	51.21-63.35
		A	0.24-0.59	25.4-37.5	4.88-6.54	53.82-62.86
		C	0.75-0.93	12.6-27.8	5.69-7.40	51.73-66.02
	CB	O	0.11-0.15	103.8-224.5	4.83-6.32	46.31-62.36
		A	0.18-0.31	86.2-152.0	4.34-6.44	49.90-62.77
		C	0.51-0.99	15.2-72.8	4.56-5.61	45.79-66.87
	HS	O	0.21-0.26	19.2-48.3	5.51-6.82	53.33-58.89
		A	0.32-0.70	18.3-27.0	5.16-6.62	53.11-58.54
		C	0.78-0.90	8.2-17.9	5.68-6.61	55.61-60.66
O		0.16-0.16	59.1-59.1	4.72-5.88	58.78-62.16	
ME		A	0.38-0.38	42.0-42.0	4.49-5.24	58.08-61.88
		C	0.72-0.72	23.6-23.6	5.42-5.60	63.06-71.75
Temperate	SHB	O	0.16-0.23	25.0-66.9	5.70-7.08	58.82-62.28
		A	0.32-0.59	13.8-50.3	5.54-6.71	55.79-62.44
		C	0.84-0.92	7.5-22.0	5.36-6.44	57.28-61.71
	SYK	O	0.21-0.21	45.9-46.7	7.23-7.77	59.33-61.05
		A	0.25-0.36	34.9-45.6	7.28-7.92	58.76-59.95
		C	0.58-1.08	6.1-22.3	7.74-8.16	58.68-61.38
	XX	O	0.11-0.19	35.6-109.6	4.64-6.35	58.92-63.85
		A	0.30-0.54	30.5-60.1	4.11-6.09	57.78-66.81
		C	0.71-1.10	7.9-42.2	4.88-6.06	54.11-70.48
	AS	O	0.19-0.56	61.6-237.3	3.70-6.32	59.18-68.21
		A	0.24-0.63	45.9-204.9	4.05-6.63	57.08-70.85
		C	0.56-1.22	19.4-61.6	4.65-6.36	57.49-73.19
GD	O	0.13-0.20	131.2-152.1	5.41-6.67	58.72-63.30	
	A	0.25-0.59	61.1-127.3	5.63-6.72	57.39-59.84	
	C	0.67-1.08	22.2-47.5	6.30-7.15	56.53-62.16	
	O	0.22-1.15	24.0-94.4	4.18-6.31	66.41-69.56	
	JF	A	0.21-0.55	40.0-180.0	4.27-5.40	66.71-70.03
		C	0.73-1.02	10.6-35.8	5.48-6.30	68.69-76.31
Warm-temperate	QF	O	0.17-0.22	113.0-139.6	5.74-6.44	47.61-65.72
		A	0.35-0.39	68.8-107.8	5.55-6.25	49.23-66.06
		C	0.59-0.88	30.2-47.3	5.96-6.41	49.89-65.65
	QL	O	0.16-0.30	73.4-173.6	5.55-7.22	59.04-64.97
		A	0.32-0.45	36.4-100.5	5.40-7.56	57.68-63.42
		C	0.73-1.20	8.1-37.5	5.60-8.11	50.17-64.64
	WYZ	O	0.11-0.18	116.9-145.7	4.12-7.07	58.90-64.72
		A	0.17-0.72	32.7-110.6	4.70-6.96	57.93-62.94
		C	0.77-0.96	15.3-22.3	5.81-6.33	60.68-66.56

		O	0.16-0.56	21.2-107.0	3.63-5.45	79.8-89.31
	AL	A	0.41-0.63	29.7-59.7	3.80-5.49	80.58-89.80
		C	0.69-0.92	24.8-45.7	4.55-5.53	79.87-91.00
		O	0.15-0.33	46.0-126.9	3.74-5.60	50.87-61.82
	DB	A	0.20-0.64	18.0-105.7	3.69-5.86	51.43-62.79
		C	0.82-1.03	8.5-26.2	4.66-5.90	51.45-74.48
		O	0.48-0.81	22.9-32.7	3.65-4.12	79.12-84.73
	DH	A	0.73-0.94	23.1-31.4	3.76-4.18	79.2-85.67
		C	0.88-1.15	15.5-17.9	3.97-4.32	79.95-85.76
	DYS	A	0.26-0.63	54.6-82.8	3.25-4.26	70.81-88.59
		C	0.53-0.97	32.4-49.4	3.58-4.31	77.30-89.18
		O	0.18-0.47	79.0-213.0	3.93-4.74	78.79-90.99
	FJS	A	0.24-0.40	66.3-197.0	4.06-4.73	79.95-92.02
		C	0.54-0.66	59.8-84.1	4.28-4.86	80.67-94.26
		O	0.15-0.24	58.5-73.1	3.39-6.76	52.55-63.91
	GGS	A	0.55-0.81	26.5-42.6	3.63-7.19	52.82-72.65
		C	1.11-1.30	13.4-29.4	4.28-8.02	48.12-75.17
		O	0.16-0.22	77.3-129.0	3.45-4.36	59.53-75.81
	JG	A	0.37-0.75	18.7-46.1	3.62-5.11	60.67-73.54
		C	0.68-0.89	14.6-19.1	4.36-5.22	55.5-74.38
	JGS	A	0.30-0.77	51.4-191.7	3.19-4.93	78.9-88.92
		C	0.75-1.66	22.1-53.6	3.92-4.76	80.07-90.10
		O	0.43-0.48	77.5-78.9	4.11-4.67	76.37-86.52
	LG	A	0.49-0.74	18.8-70.3	4.26-4.71	79.38-87.29
		C	0.82-0.89	29.8-37.2	4.58-4.84	81.52-88.71
		O	0.18-0.36	74.5-173.1	3.59-3.91	54.95-69.98
	LJ	A	0.21-0.59	28.3-131.7	3.72-5.80	58.03-81.09
		C	0.85-1.02	19.5-40.1	3.83-6.34	59.00-82.45
		O	0.18-0.79	44.7-227.6	3.68-4.76	64.69-79.82
	NL	A	0.45-0.85	40.8-109.4	3.49-4.46	64.97-80.51
		C	0.83-1.12	14.7-43.5	4.12-4.61	66.8-83.91
		O	0.11-0.56	31.73-187.5	4.13-6.58	65.22-74.39
	SN	A	0.22-0.63	33.5-136.2	3.67-7.35	64.35-76.16
		C	0.55-0.96	20.5-61.3	4.16-6.78	68.13-81.39
		O	0.31-0.67	42.9-130.7	3.62-5.78	80.43-94.92
	SWDS	A	0.65-0.97	18.3-85.6	3.33-7.16	80.44-95.64
		C	0.84-1.52	17.3-41.0	3.69-4.28	80.69-95.81
		O	0.36-0.66	50.3-86.4	3.80-5.93	69.04-81.79
	TM	A	0.64-0.66	49.1-70.6	3.71-4.77	72.74-82.35
		C	0.92-0.92	29.9-29.9	4.58-4.66	74.97-75.77
	WGS	A	0.40-0.92	53.3-118.8	3.95-5.34	73.34-87.58
		C	0.55-1.00	37.6-101.5	3.90-5.67	70.28-87.65
	Tropical	A	0.71-0.86	49.7-73.7	3.52-3.96	84.89-92.80
		C	1.04-1.38	25.2-32.2	3.98-4.42	85.40-93.40

645 AL, Mt. Ailao; AS, Mt. Ao; BCW, Mt. Baicaowa; CB, Mt. Changbai; DB, Mt. Dabie; DH, Mt. Dinghu;  
646 DX, Mt. Daxinganling; DYS, Mt. Daiyun; FJS, Mt. Fanjing; GD, Mt. Guandi; GGS, Mt. Gongga; HS,  
647 Mt. Han; JF, Mt. Jifeng; JG, Mt. Jiugong; JGS, Mt. Jinggang; LJ, Mt. Luoji; LG, Mt. Leigong; LJ, Mt.  
648 Luoji; ME, Mt. Maoer; NL, Mt. Nanling; QF, Mt. Qingfengxia; QL, Mt. Qinling; SHB, Mt. Saihanba;  
649 SN, Mt. Shennongjia; SWDS, Mt. Shiwandashan; SYK, Mt. Suyukou; TM, Mt. Tianmu; WGS, Mt.  
650 Wugong; WYZ, Mt. Wuyuezhai; WZS, Mt. Wuzhi; XX, Mt. Xiaoxinganling; BD, bulk density; CIA,  
651 chemical index of alteration.



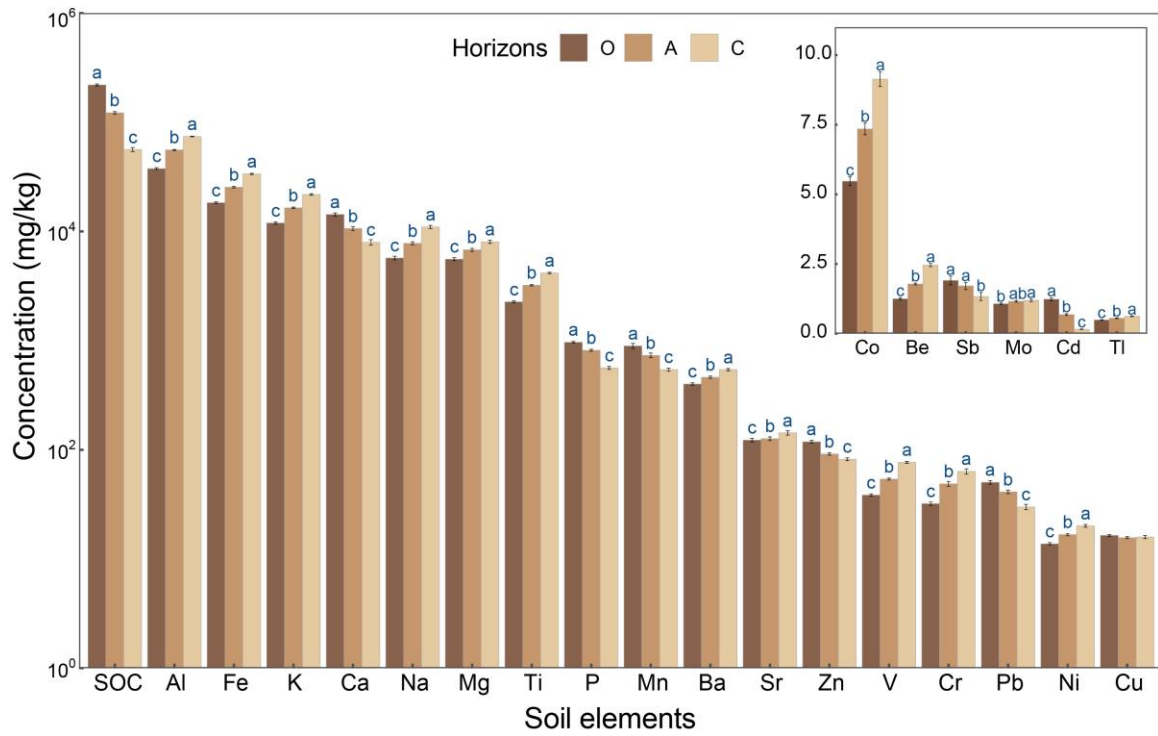
652  
 653 **Fig. 1** Geographic distribution of the 30 China's mountains. AL, Mt. Ailao; AS, Mt. Ao; BCW, Mt.  
 654 Baicaowa; CB, Mt. Changbai; DB, Mt. Dabie; DH, Mt. Dinghu; DX, Mt. Daxinganling; DYS, Mt.  
 655 Daiyun; FJS, Mt. Fanjing; GD, Mt. Guandi; GGS, Mt. Gongga; HS, Mt. Han; JF, Mt. Jifeng; JG, Mt.  
 656 Jiugong; JGS, Mt. Jinggang; LJ, Mt. Luoji; LG, Mt. Leigong; LJ, Mt. Luoji; ME, Mt. Maoer; NL, Mt.  
 657 Nanling; QF, Mt. Qingfengxia; QL, Mt. Qinling; SHB, Mt. Saihanba; SN, Mt. Shennongjia; SWDS, Mt.  
 658 Shiwandashan; SYK, Mt. Suyukou; TM, Mt. Tianmu; WGS, Mt. Wugong; WYZ, Mt. Wuyuezhai; WZS,  
 659 Mt. Wuzhi; XX, Mt. Xiaoxinganling.



660

661 **Fig. 2** Frequency distribution of soil elements across the China's mountains. Red curve on each histogram  
 662 represents the fitted normal distribution. The statistical parameters of the corresponding element are  
 663 annotated in the upper left of each sub-figure.

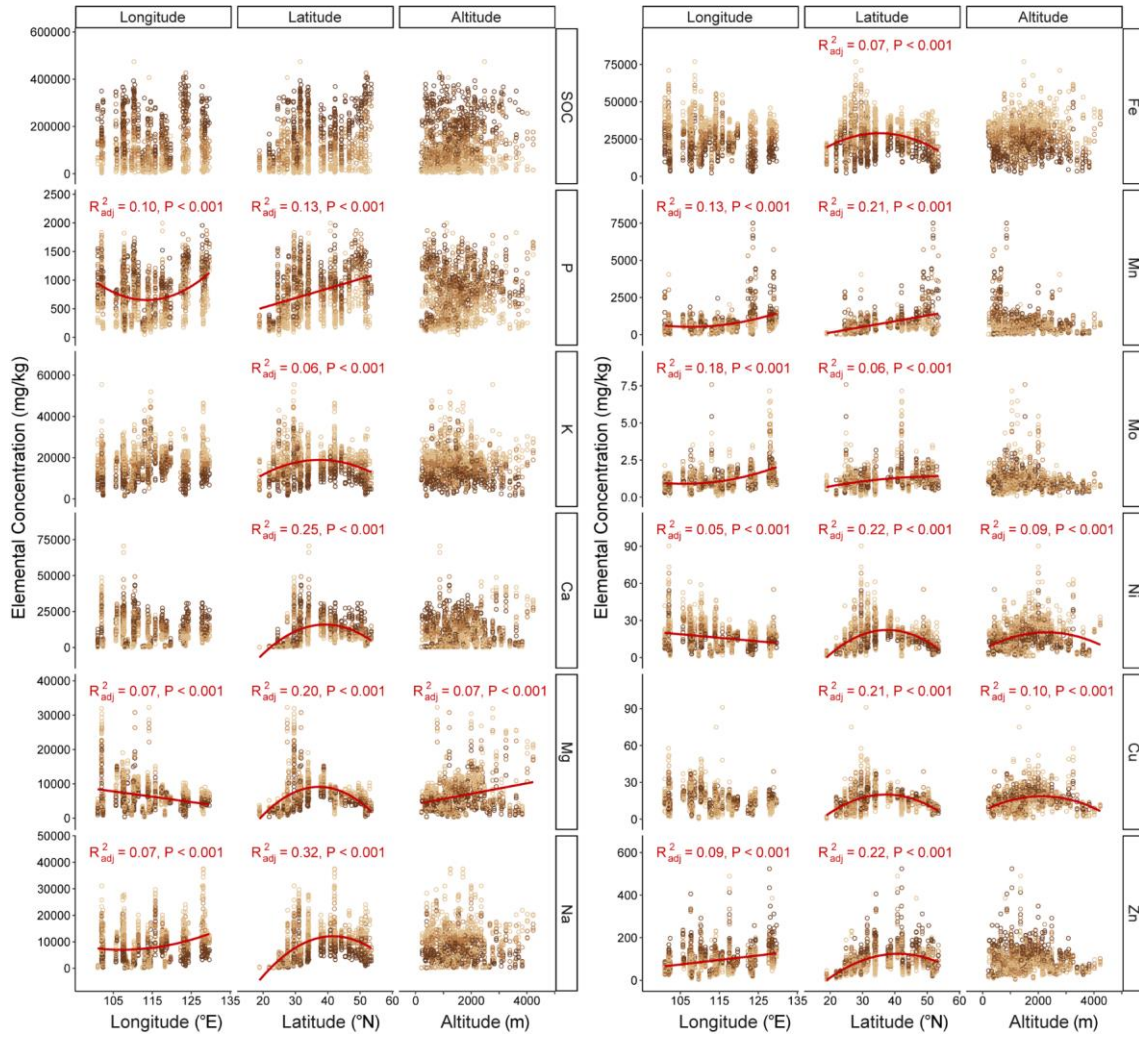




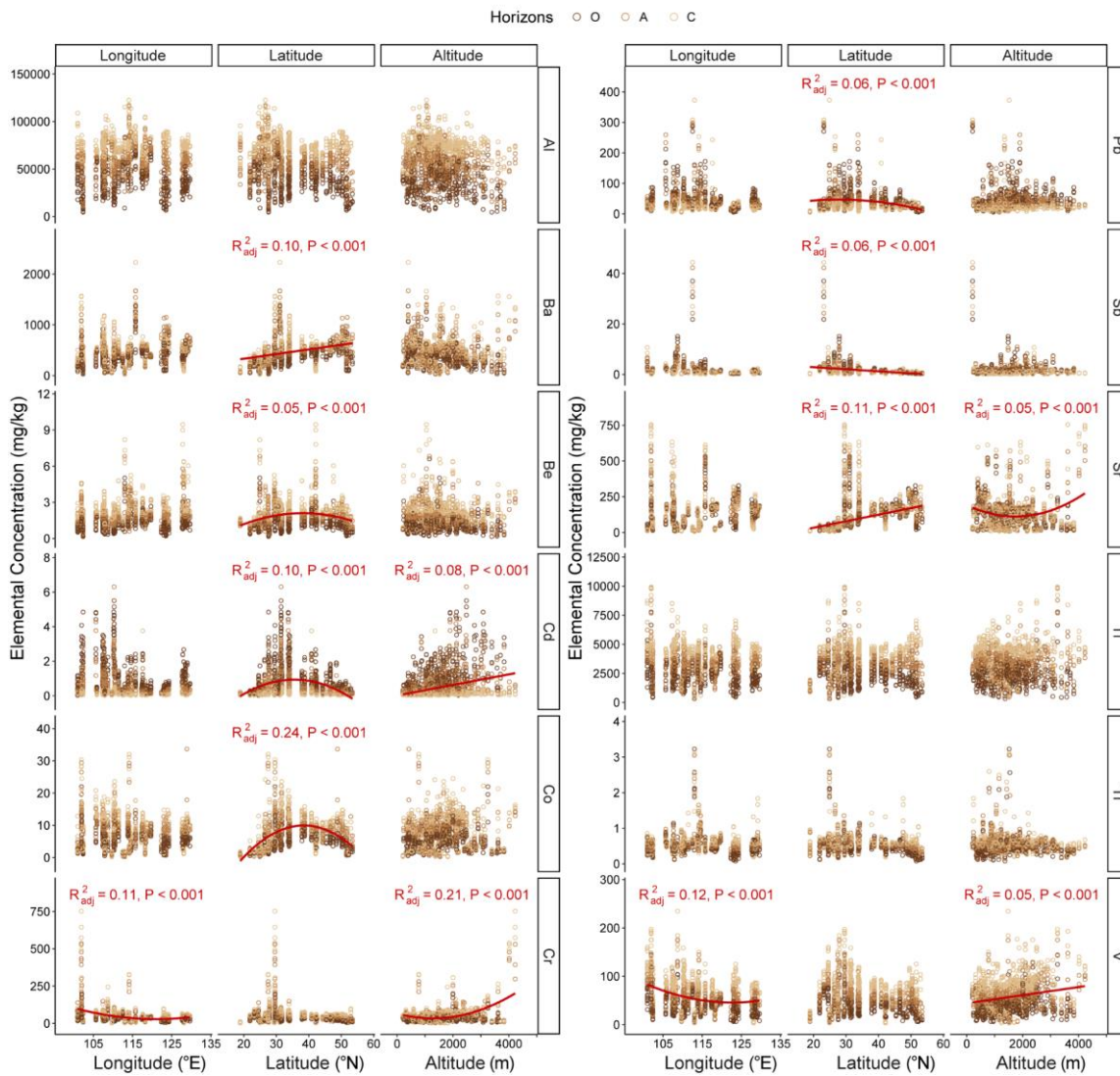
664

665 **Fig. 3** Mean concentrations of 24 elements across different soil horizons. Lowercase letters indicate  
 666 significant differences in each element among soil horizons ( $p < 0.05$ ), and error bars represent the  
 667 standard error.

Horizons ○ O ○ A ○ C



668



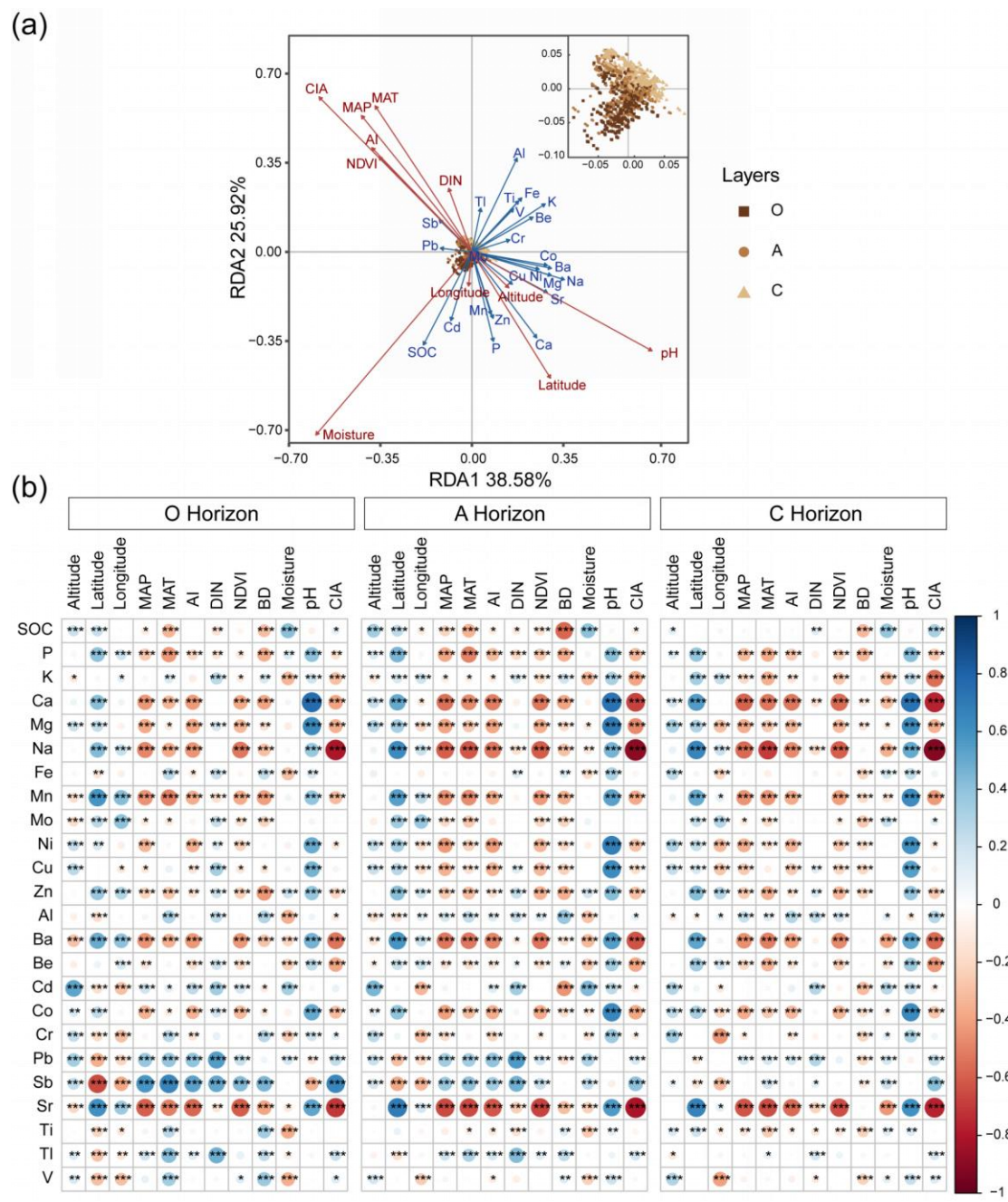
669

670

671

672

**Fig. 4** Spatial distribution of soil element concentrations across latitude, longitude, and altitude. The colors of the dots represent different soil horizons. Solid red lines represent the fitting relationships of elemental concentrations with latitude, longitude, and altitude ( $p < 0.05$ ).  $R^2$  less than 0.05 are not shown.



673

674

**Fig. 5** The environmental factors influencing the elemental concentrations in the soils. (a)

675

Redundancy analysis (RDA) shows the relationships of soil elements with environmental factors

676

across soil horizons. The inserted figure shows the distribution of samples along the axes. (b)

677

Correlation heatmap shows the correlation between soil element concentrations and environmental

678

variables in each soil horizon. The color and circle size represent the correlation coefficient, and \*

679

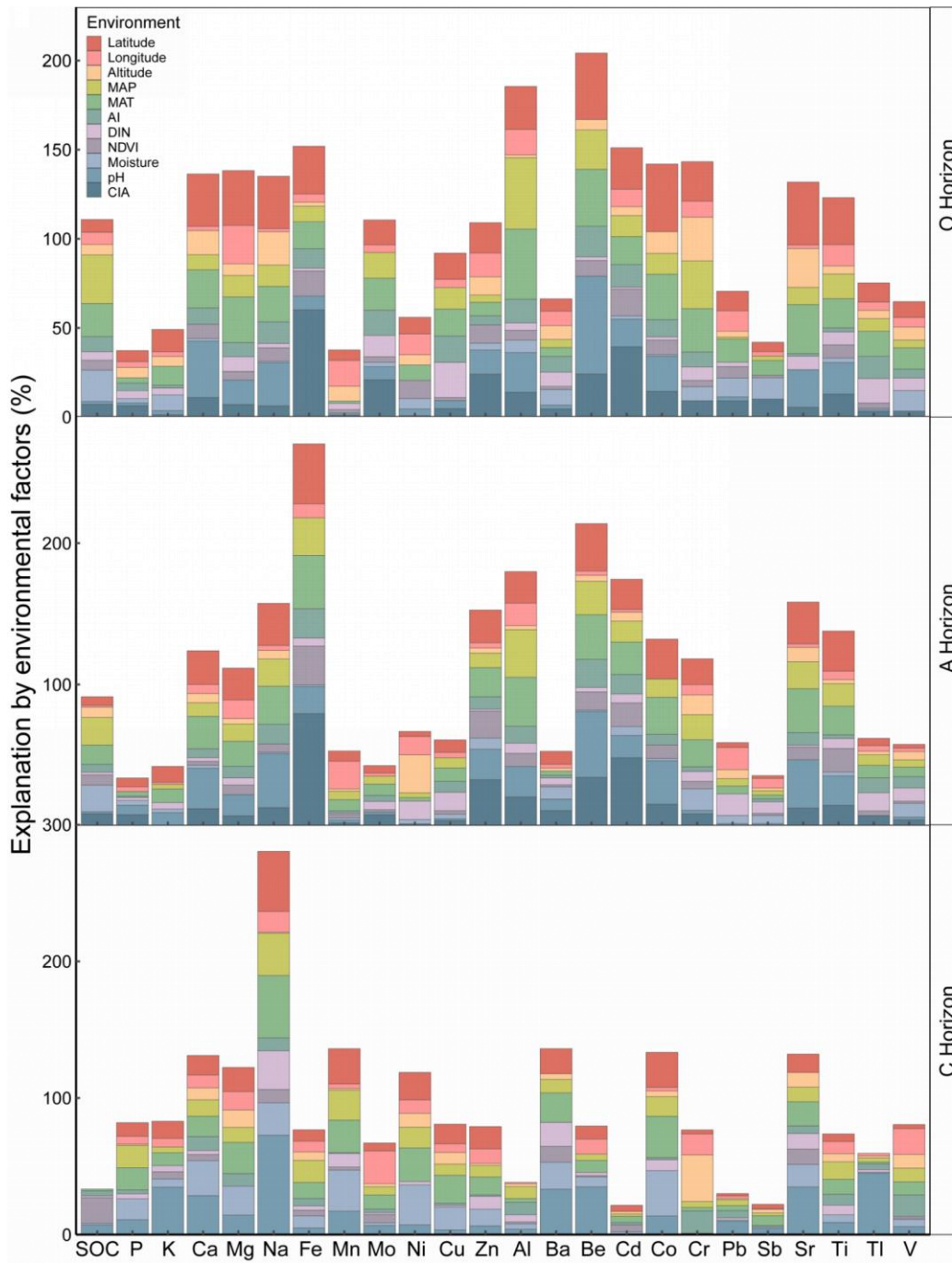
indicates statistical significance ( $p < 0.05$ ). SOC, soil organic carbon; MAP, mean annual

680

precipitation; MAT, mean annual temperature; AI, aridity index; DIN, dissolved inorganic nitrogen;

681

NDVI, normalized difference vegetation index; BD, bulk density; CIA, chemical index of alteration



682

683

**Fig. 6** Explanation of elemental variation by environmental factors based on regression modelling.

684

Columns with different colors represent different environmental variables. Total height of each bar

685

indicates the cumulative explanatory power. MAP, mean annual precipitation; MAT, mean annual

686

temperature; AI, aridity index; DIN, dissolved inorganic nitrogen; NDVI, normalized difference

687

vegetation index; CIA, chemical index of alteration